

**Lacustrine leaf wax hydrogen isotopes indicate strong regional climate**

**W. C. Daniels<sup>1,2</sup>, J. M. Russell<sup>1</sup>, C. Morrill<sup>3,4</sup>, W. M. Longo<sup>1</sup>, A. E. Giblin<sup>2</sup>, P. Holland-Stergar<sup>1</sup>, J. M. Welker<sup>5,6</sup>, X. Wen<sup>7</sup>, A. Hu<sup>8</sup>, Y. Huang<sup>1</sup>**

<sup>1</sup>Department of Earth, Environment and Planetary Science; Brown University; 324 Brook St., Providence, RI, 02912.

<sup>2</sup>The Ecosystem Center; Marine Biological Laboratory; 7 MBL St., Woods Hole, MA, 02543.

<sup>3</sup>Cooperative Institute for Research in Environmental Sciences; University of Colorado; Boulder, CO, 80309.

<sup>4</sup>National Centers for Environmental Information, NOAA, 325 Broadway, Code E/NE33, Boulder, CO 80305.

<sup>5</sup>Department of Biological Sciences, University of Alaska, Anchorage; Anchorage, AK.

<sup>6</sup>Ecology and Genetics Research Unit, University of Oulu, Finland & UArctic.

<sup>7</sup>Department of Atmospheric and Oceanic Sciences, Peking University; Beijing China, 100871.

<sup>8</sup>Climate and Global Dynamics Laboratory, National Center for Atmospheric Research, Boulder, CO 80305.

Corresponding author: William Daniels ([william\\_daniels@alumni.brown.edu](mailto:william_daniels@alumni.brown.edu)); ORCID: 0000-0002-3424-2273

## 26    **Abstract**

27           The Late-Quaternary climate of Beringia remains unresolved despite the region's  
28    role in modulating glacial-interglacial climate and as the likely conduit for human  
29    dispersal into the Americas. Here, we investigate Beringian temperature change using an  
30    ~32,000-year lacustrine record of leaf wax hydrogen isotope ratios ( $\delta^2\text{H}_{\text{wax}}$ ) from Arctic  
31    Alaska. Based on Monte Carlo iterations accounting for multiple sources of uncertainty,  
32    the reconstructed summertime temperatures were ~3 °C colder (range: -8 to +3 °C)  
33    during the Last Glacial Maximum (LGM; 21-25 ka) than the pre-industrial era (PI; 2-0.1  
34    ka). This ice-age summer cooling is substantially smaller than in other parts of the Arctic,  
35    reflecting altered atmospheric circulation and increased continentality which weakened  
36    glacial cooling in the region. Deglacial warming was punctuated by abrupt events that are  
37    largely synchronous with events seen in Greenland ice cores that originate in the North  
38    Atlantic but which are also controlled locally, such as by the opening of the Bering Strait  
39    between 13.4 and 11 ka. Our reconstruction, together with climate modeling experiments,  
40    indicates that Beringia responds more strongly to North Atlantic freshwater forcing under  
41    modern-day, open-Bering Strait conditions than under glacial conditions. Furthermore, a  
42    2 °C increase (Monte Carlo range: -1 to +5 °C) over the anthropogenic era reverses a 6  
43    °C decline (Monte Carlo range: -10 to 0 °C) through the Holocene, indicating that recent  
44    warming in Arctic Alaska has not surpassed peak Holocene summer warmth.

## 46    **Keywords**

47    Holocene, Last Glacial Maximum, Paleoclimatology, Arctic Alaska, Continental  
48    biomarkers, Leaf wax hydrogen isotopes

## 50    **1 Introduction**

51           During the last glacial termination, the Arctic experienced some of the most  
52    extreme temperature changes known in recent geologic time. In the North Atlantic  
53    region, this includes up to 23 °C of warming from 25 ka to present (Dahl-Jensen et al.,  
54    1998) and abrupt changes on the order of 4-14 °C such as the Bølling-Allerød (BA), and  
55    the Younger Dryas (YD) (Johnsen et al., 1992; Groote et al., 1993; Severinghaus and  
56    Brook, 1999; Buizert et al., 2014). The magnitude and rate of these changes are linked to

57 changes in the strength of the Atlantic meridional overturning circulation (AMOC) and  
58 feedbacks from sea ice (Broecker et al., 1989; Li et al., 2005) that cause temperature  
59 changes to be larger than anywhere else on earth – a phenomenon known as “Arctic  
60 Amplification” (Shakun and Carlson, 2010). Based on paleoclimate records, Miller et al.  
61 (2010) estimate that Arctic temperature change exceeds that of the northern hemisphere  
62 by a factor of 3-4. This finding, however, is weighted heavily by the estimate of Last  
63 Glacial Maximum (LGM) cooling which has high uncertainty as it is derived primarily  
64 from the Greenland ice core borehole temperatures (Dahl-Jensen et al., 1998; Miller et  
65 al., 2010) which may not represent temperature changes over the entire Arctic (Shakun  
66 and Carlson, 2010). Additional continuous paleotemperature records extending through  
67 the LGM are needed to better understand the spatiotemporal variations in Arctic  
68 Amplification, and its underlying physics.

69 Eastern Beringia, the region today encompassing Alaska and the Yukon Territory,  
70 also experienced dramatic environmental changes during the last glacial-interglacial  
71 transition. Several paleoenvironmental archives extend through the last glacial period,  
72 owing to the lack of regional glaciation during the LGM. Major changes included the  
73 submergence of the Bering Land Bridge, the expansion of peat soils (Jones and Yu, 2010)  
74 as well as trees and shrubs (Eisner and Colinvaux, 1992; Oswald et al., 1999; Mann et al.,  
75 2010), retreat of mountain glaciers (Hamilton, 2003; Pendleton et al., 2015), permafrost  
76 degradation (Mann et al., 2010), the loss of megafauna (Mann et al., 2013), and the  
77 appearance of humans (Goebel et al., 2008). Questions remain, however, about the  
78 temperature changes during the deglacial period. Some Arctic Alaskan pollen-based  
79 estimates suggest LGM temperatures were actually warmer than present (Bartlein et al.,  
80 2011). Lower sea levels increased the continentality of Alaska and may have weakened  
81 summertime cooling (Mann et al., 2001; Bartlein et al., 2015). Climate models further  
82 predict that Laurentide Ice Sheet (LIS) orography steered warm air into Alaska during the  
83 LGM maintaining relatively mild or even warmer temperatures relative to the present  
84 (Broccoli and Manabe, 1987; Otto-Bliesner et al., 2006; Bartlein et al., 2011; Tierney et  
85 al., 2020). However, pollen-based temperature reconstructions are limited because  
86 Pleistocene ecosystems of Beringia have no modern analog, while different climate

87 models predict different, and often opposite, temperature changes in Arctic Alaska in  
88 response to changes in LIS height (Figure S1), calling this mechanism into question.

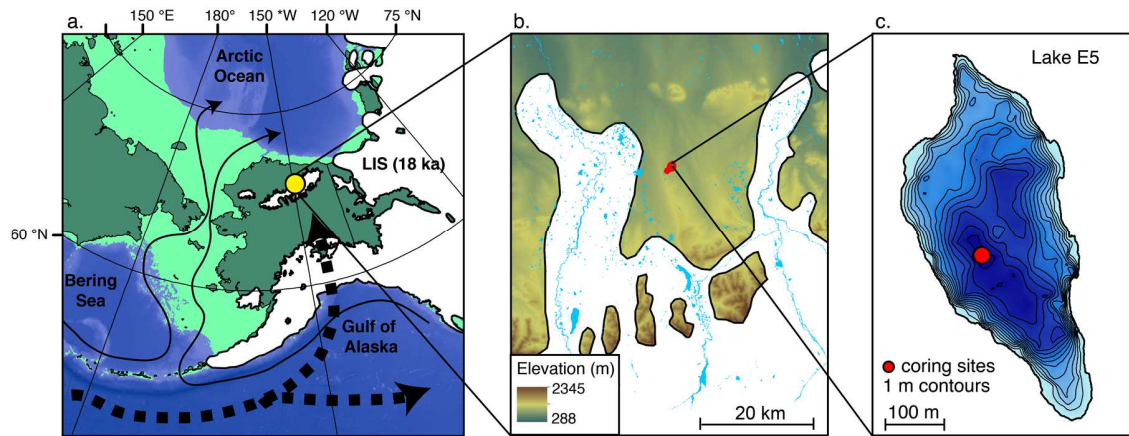
89         Within the last glacial termination, much of the Arctic experienced abrupt climate  
90 events associated with Heinrich Stadial 1 (HS1), the BA, and the YD. In Eastern  
91 Beringia, evidence for BA-YD climate reversals is found in both marine (Praetorius and  
92 Mix, 2014) and terrestrial records (Engstrom et al., 1990; Epstein, 1995; Mann et al.,  
93 2002; Meyer et al., 2010; Young et al., 2019), although several locations show no YD  
94 signal (Kurek et al., 2009b). The magnitude of temperature changes during these abrupt  
95 transitions is not tightly constrained in Alaska, but is thought to be weaker than in the  
96 North Atlantic (Hu et al., 2006; Graf and Bigelow, 2011). In addition to these millennial-  
97 scale events, resubmergence of the Bering land bridge and establishment of Bering Strait  
98 throughflow between 13.4 ka and 11.0 ka (Keigwin et al., 2006; England and Furze,  
99 2008; Jakobsson et al., 2017; Pico et al., 2020) likely had considerable influence on local  
100 Beringia climate. Sites adjacent to the Bering Strait cooled in summer and warmed in  
101 winter in response to an increasingly maritime climate (Mann et al., 2001; Bartlein et al.,  
102 2015), although the spatial ramifications of this transition are unconstrained. This effect  
103 may have been partially offset by the initiation of north-flowing ocean currents and heat  
104 transport from the North Pacific into the Western Arctic, warming broader Beringia (Hu  
105 et al., 2012), a hypothesis which requires more investigation. Bering Strait status is also  
106 proposed to modulate the North Pacific circulation response to deglacial freshwater  
107 release events in the North Atlantic (Hu et al., 2012). For example, during HS1 (~15-18  
108 ka), collapse of AMOC is associated with an invigoration of Pacific Meridional Oceanic  
109 Circulation (PMOC) (Okazaki et al., 2010; Maier et al., 2018), minimizing or even  
110 reversing temperature changes in the North Pacific relative to the North Atlantic  
111 (Sarnthein et al., 2006). Warm sea surface temperatures during HS1 may have influenced  
112 continental Beringia, as suggested by chironomid-inferred warming from 17-14 ka at  
113 Zagoskin Lake in Alaska (Kurek et al., 2009a), although more records are needed to  
114 confirm this.

115         Here, we generate a centennially-resolved record of temperature change from the  
116 northern foothills of the Brooks Range mountains (68.643 °N, 149.458 °W, Figure 1) to  
117 examine the amplitude and causes of temperature changes from Arctic Alaska during the

118 LGM, the last deglaciation, and the Holocene. This new dataset, alongside paleoclimate  
 119 data-model comparisons, provide new insight into the large-scale and regional controls  
 120 on temperature change in this part of the Arctic.

121

## 122 2 Materials and Methods



123

124 **Figure 1.** a) Map of Beringia with ice extent 18,000 calendar years before present (18 ka)  
 125 (Dyke, 2004) and E5 study lake (yellow dot). Dark and light green show modern and  
 126 approximate LGM coastline, respectively. Bold dashed arrows represent the LIS-  
 127 orography forced northward advection of subpolar air into Alaska as simulated in  
 128 CCSM3 (Otto-Bliesner et al., 2006). Solid arrows are modern surface currents through  
 129 the Bering Strait (Stabeno et al., 1999). b) study area showing surface waters, the Lake  
 130 E5 watershed (red), and the maximum glacier extent of the late-Wisconsin glaciation  
 131 (Manley and Kaufman, 2002). c) Lake E5 bathymetry (Toolik GIS, 2019) and coring  
 132 sites.

133

### 134 2.1 Lake Setting and Core Chronology

135 Lake E5, located in Alaska's North Slope (Figure 1), is a glacial lake containing  
 136 sediments extending through the LGM (Eisner and Colinvaux, 1992), providing an  
 137 extraordinary opportunity to examine deglacial climate change in the Western Arctic.  
 138 Meteorological observations at the nearby Toolik Field Station, approximately 5 km to  
 139 the west, show that mean annual temperature averages  $-8.5^{\circ}\text{C}$ , summer temperatures  
 140 (JJA) average  $9^{\circ}\text{C}$ , and precipitation averages 312 mm with 60% falling during summer  
 141 (Cherry et al., 2014).

142 The study lake is situated on glacial deposits dating to 780-125 ka (Hamilton,  
 143 2003). It is 12 m deep and typically ice-free from early June to mid-September. Gravity  
 144 cores were retrieved from a boat in 2011 and 2012, and in May, 2014, overlapping

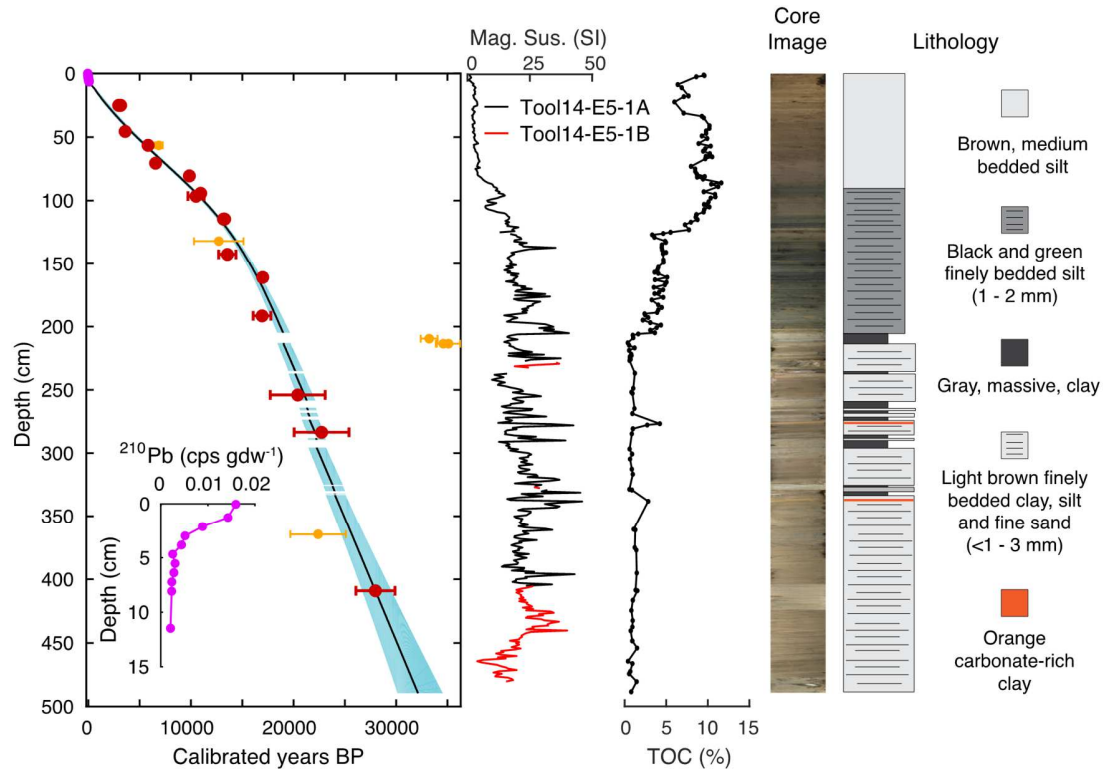
145 sediment cores were recovered using a Bolivia and modified Livingstone square-rod  
146 piston corer through the ice from the deepest point in the lake. Core images and magnetic  
147 susceptibility (MS) profiles were generated with a GeoTek multisensor core logger  
148 (MSCL).

149 The previously-published chronology for the Lake E5 composite core (Figure 2)  
150 is based on  $^{210}\text{Pb}$  (Table S1) and 16 radiocarbon dates (Table S2) (Vachula et al., 2019;  
151 Longo et al., 2020).  $^{210}\text{Pb}$  was measured on core Tool12-E5-1B using gamma  
152 spectroscopy (Appleby et al., 1986). Ages and age uncertainty were modeled using the  
153 constant rate of supply (Appleby and Oldfield, 1978; Binford, 1990), and these data were  
154 incorporated into the composite core age model as non-radiocarbon age constraints.

155 The materials analyzed for radiocarbon consist of both plant and aquatic insect  
156 fragments (Table S2), both of which may be prone to over-estimating depositional ages in  
157 Arctic lakes. Terrestrial components can incur pre-aging on the landscape prior to  
158 transport into the lake (Abbott and Stafford Jr, 1996). To address this, Oswald et al.  
159 (2005) suggested that small, non-woody plant fragments are least prone to landscape pre-  
160 aging and provide the most reliable depositional ages. In the Lake E5 cores, the plant-  
161 derived radiocarbon dates come from ultrasmall fragments of grasses and moss. Recently  
162 developed spectrometry techniques for ultrasmall samples (Shah Walter et al., 2015)  
163 were used for the analyses.

164 Where terrestrial plant fragments were absent, aquatic organisms were measured  
165 for radiocarbon. Aquatic insect remains can overestimate sediment deposition ages in  
166 Arctic lakes due to incorporation of  $^{14}\text{C}$ -depleted methane, DOC, or DIC into aquatic  
167 food webs (Abbott and Stafford Jr, 1996; Wooller et al., 2012). We tested for this effect  
168 by independently dating insect eggs and plant fragments from the 24.5-25.5 cm horizon,  
169 and insect eggs and daphnia ephippia from the 113.5-115.5 cm horizon (Table S2). No  
170 significant age differences are observed between organic materials. This, together with  
171 recent findings that radiocarbon ages of lake-derived methane from Northern Alaska is  
172 surprisingly young (Elder et al., 2018), indicate that incorporation of pre-aged carbon into  
173 aquatic organisms is minimal and justifies the use of aquatic macrofossils in the age  
174 model.

175 Ages were modeled using the Clam version 2.2 (Blaauw, 2010) with IntCal13  
 176 (Reimer et al., 2013). The Clam settings were: type=4, wgts=1, smooth=0.6. A series of  
 177 discrete sedimentary beds are modeled as slump events in the Clam software, and leaf  
 178 wax isotope measurements were omitted from these intervals.



179  
 180 **Figure 2.** Age model and lithologic profiles for the Lake E5 sediment core. Radiocarbon  
 181 ages are calibrated using the Intcal13 calibration curve (Reimer et al., 2013). The spline  
 182 and 95% error envelope were modeled in clam.R software (Blaauw, 2010). Orange points  
 183 are outliers and not included in the CLAM model. The magenta inset curve shows  $^{210}\text{Pb}$   
 184 concentration measured using gamma spectroscopy. Instantaneous deposition events are  
 185 shown as gaps.  
 186

## 187 2.2 Leaf Wax Hydrogen Isotope Analysis

188 Hydrogen isotope ratios of terrestrial leaf waxes ( $\text{C}_{28}$  *n*-acid; hereafter  $\delta^2\text{H}_{\text{wax}}$ )  
 189 were measured in Lake E5 sediments as a proxy for changes in past  $\delta^2\text{H}_{\text{precipitation}}$  and  
 190 climate. Lipids were extracted from 1-5 g of dry sediment using a Dionex accelerated  
 191 solvent extractor with 9:1 dichloromethane:methanol. Total lipid extracts were separated  
 192 using aminopropyl silica gel chromatography with 2:1 dichloromethane:isopropanol and  
 193 4% acetic acid in ether as eluents. Acid fractions were then methylated overnight at 60 °C

194 in acidified methanol of known isotopic composition. Further purification of fatty acid  
195 methyl esters (FAMES) was performed with silica gel chromatography with  
196 dichloromethane and hexane as eluents.

197 Hydrogen isotope ratios of FAMES were analyzed on a Thermo Finnegan Delta  
198 XL GC-IRMS at Brown University. Each sample was injected at least twice, targeting the  
199 *n*-C<sub>28</sub> acid to be in the range of 3-5 volts. The  $\delta^2\text{H}$  values are reported relative to  
200 VSMOW in delta notation, and analytical uncertainties are reported in Table S3.  $\delta^2\text{H}_{\text{wax}}$   
201 values are mathematically corrected for the methyl groups added during derivatization.

202

### 203 2.3. Temperature estimation

204 Previous quantitative reconstructions of  $\delta^2\text{H}_{\text{precipitation}}$  from measurements of  
205  $\delta^2\text{H}_{\text{wax}}$  have demonstrated the need to account for glacial-interglacial changes in oceanic  
206  $^2\text{H}/^1\text{H}$  ratios (Konecky et al., 2016). We correct for this effect across the last glacial  
207 termination by subtracting the  $\delta^2\text{H}_{\text{ocean}}$  anomaly from the measurements of  $\delta\text{D}_{\text{wax}}$ . The  
208  $\delta^2\text{H}_{\text{ocean}}$  anomaly is determined by assuming LGM ocean was 1‰ enriched in  $\delta^{18}\text{O}$   
209 relative to today (Schrag et al., 1996), scaling the 1‰ glacial-interglacial change to the  
210 foramanifera-inferred changes in  $\delta^{18}\text{O}$  (Lisiecki and Raymo, 2005), then converting to  
211  $\delta^2\text{H}$  by multiplying by 8.

212 Additionally, determination of  $\delta^2\text{H}_{\text{precipitation}}$  from  $\delta^2\text{H}_{\text{wax}}$  is improved by  
213 accounting for changes in terrestrial plant assemblages (Feakins, 2013; Konecky et al.,  
214 2016), as the  $^2\text{H}/^1\text{H}$  fractionation between water and lipids ( $\epsilon_{\text{app}}$ ) varies among plant types  
215 (Sachse et al., 2012; Gao et al., 2014). At Lake E5, the Holocene is characterized by  
216 greater abundance of dicot shrubs, particularly of the genera *Betula*, *Salix*, and *Alnus*,  
217 whereas during the LGM, grasses (*Poaceae*) were relatively abundant (Livingstone,  
218 1955; Eisner and Colinvaux, 1992; Abbott et al., 2010). During the glacial termination,  
219 transient peaks in *Artemesia* and sedges of the *Cyperaceae* family are evident around 16  
220 and 11-15 ka, respectively (Eisner and Colinvaux, 1992; Abbott et al., 2010).

221 Despite the recognition of variable  $\epsilon_{\text{app}}$  among Arctic plants (Wilkie et al., 2012;  
222 Daniels et al., 2017; Daniels et al., 2018; Berke et al., 2019; Dion-Kirschner et al., 2020;  
223 O'Connor et al., 2020), there are few  $\delta^2\text{H}_{\text{wax}}$  studies which attempt to correct for  
224 vegetation changes in the Arctic (Nichols et al., 2014).  $^2\text{H}/^1\text{H}$  fractionation estimates are



not available for all Arctic taxa, so here we follow methods of Feakins (2013) and Nichols et al. (2014) by broadly grouping plant taxa, and applying an end-member mixing model to estimate past  $\epsilon_{app}$  values (Figure S3). The broad plant groupings include monocot and dicot plants, as in Nichols et al. (2014), and the  $\epsilon_{app}$  end-members are scaled to the fraction of monocot and dicot represented in the previously documented pollen spectra from Lake E5 (previously called "Oil Lake"; Eisner and Colinvaux, 1992) which was depth-correlated to our stratigraphy based on organic carbon profiles and a distinct marker bed dating to the beginning of the deglaciation. Generally, monocotyledonous plants fractionate more strongly than dicotyledonous plants (Gao et al., 2014).

Several estimates of  $\epsilon_{app}$  are available from the Arctic for specific plants taxa and for integrated sediments (Wilkie et al., 2012; Daniels et al., 2017; Berke et al., 2019; McFarlin et al., 2019). We opt to use local landscape-scale  $\epsilon_{app}$  values determined from a 24-lake surface sediment training set in the Alaskan tundra which includes Lake E5 (Daniels et al., 2017). More negative  $\epsilon_{app}$  values for  $C_{28}$   $n$ -acids are associated with a predominance of wet sedge tundra or grasses while lakes within dicot-dominated forb/shrub tundra exhibit weaker fractionation. Based on a regression between  $C_{28}$   $\epsilon_{app}$  and landcover type, we select endmember  $\epsilon_{app}$  values of -135 ‰ ( $1\sigma = 20\%$ ) to represent monocot taxa and -96 ‰ ( $1\sigma = 16\%$ ) for dicot taxa. These end member choices are comparable to fractionation values for modern plants. The  $\epsilon_{app}$  of arctic shrubs, including *Betula nana*, *Salix* sp., and others, ranges from -96‰ to -108‰ (Daniels et al., 2017; Dion-Kirschner et al., 2020; O'Connor et al., 2020). Fractionation factors of graminoids are more variable –  $C_{28}$   $n$ -acid of *Eriophorum vaginatum* (monocot sedge) in Alaska exhibits  $\epsilon_{app}$  of -159 ‰ (Daniels et al., 2017), whereas *Carex* sp. analyzed in Greenland had  $\epsilon_{app}$  of just -98 ‰ (Dion-Kirschner et al., 2020). Nichols et al. (2014) used endmember of -114 ‰ and -159 ‰, somewhat more negative than our choices but with a comparably amount of spread between them, such that the correction would be similar in a relative sense. Inclusion of species-level endmembers or broader geographic calibration may improve the mixing model, although the differentiation between monocots and dicots clearly elucidated by Gao et al. (2014) and Sachse et al. (2012) should provide a first-order correction for changing plant assemblages.

255           There are several assumptions inherent in the quantitative conversion from  $\delta^2\text{H}_{\text{wax}}$   
256 to  $\delta^2\text{H}_{\text{precipitation}}$ . First, we assume that the  $\text{C}_{28}$  *n*-acids are derived from land plants  
257 (Chikaraishi and Naraoka, 2007) and are geochemically stable in sediments (Yang and  
258 Huang, 2003). While long chain ( $>\text{C}_{24}$ ) *n*-acids can also be produced by aquatic  
259 vegetation, terrestrial tundra plants produce considerably higher concentrations of *n*-  
260 alkanes and *n*-acids than submerged and emergent aquatic vegetation of tundra lakes  
261 (Dion-Kirschner et al., 2020). Furthermore, our observations during repeated sampling of  
262 the lake by the Toolik Long-Term Ecological Research suggest that macrophytes are not  
263 particularly abundant and the littoral zone is characterized by cobbles and soft sediment.  
264 The low light penetration and extremely oligotrophic status of Lake E5 (Daniels et al.,  
265 2015) suggests that terrestrial sources dominate the long chain waxes.

266           Additionally, vegetation corrections are likely imperfect because of uncertainty in  
267 the pollen-wax production ratios among different plants. For example, pollen assemblage  
268 has little predictive capacity on leaf wax  $\delta^2\text{H}$  in the tropical Pacific island lakes (Ladd et  
269 al., 2021); an assessment relating pollen directly to leaf wax signatures is needed for the  
270 Arctic. Furthermore, pollen assemblages from arctic lakes may record regional signals  
271 and exhibit lags in response to climate change (Crump et al., 2019), and the methods here  
272 assume that the leaf waxes and pollen both respond similarly and rapidly to climate  
273 change. Nonetheless, a pollen-based approach has been used previously with success  
274 (Feakins, 2013), despite introducing a high degree of quantitative uncertainty (Dion-  
275 Kirschner et al., 2020).

276           To estimate temperature from  $\delta^2\text{H}_{\text{precipitation}}$ , we use the temperature- $\delta^2\text{H}_{\text{precipitation}}$   
277 relationship determined from 20 years of precipitation monitoring at the Toolik Field  
278 Station (Klein et al., 2015), approximately 5 km west of and at a similar elevation to Lake  
279 E5. Over the 20 years of monitoring, precipitation sampling for  $^{18}\text{O}/^{16}\text{O}$  and  $^2\text{H}/^1\text{H}$  was  
280 opportunistic, included all seasons, including winter, made possible by researchers and  
281 field staff on site 12 months per year. Specific precipitation events were neither targeted  
282 nor avoided. Average daily temperatures during days when precipitation was collected  
283 were extracted from the Toolik Environmental Data Center (Toolik Environmental Data  
284 Center Team, 2016). We tested the  $\delta^2\text{H}$ -temperature relationship further using an isotope-  
285 enabled version of the Community Atmosphere Model (IsoCAM) to examine changes in

286 the slope of the  $\delta^2\text{H}_{\text{precipitation}}\text{-T}$  relationship at 1000-year time slices over the past 20 kyr  
287 in Alaska, as the relationship between these variables might be expected to change with  
288 major moisture source changes (Tharammal et al., 2013; Liu et al., 2014; Thomas et al.,  
289 2014). Monthly temperatures were extracted from each time slice for 40 years from 6  
290 grid cells that cover Northern Alaska, and we analyzed the relationship between  
291 temperature and  $\delta^2\text{H}_{\text{precipitation}}$  on these data.

292 All vegetation corrections and temperature conversions were performed in a  
293 Monte Carlo simulation in order to propagate uncertainty estimates of the  $\delta^2\text{H}_{\text{wax}}$   
294 measurements (average  $1\sigma = 1.3\text{‰}$ , Table S3), the pollen-inferred vegetation  
295 assemblages (ie. fraction monocot and fraction dicot;  $1\sigma$  prescribed at 0.05),  $^2\text{H}/^1\text{H}$   
296 fractionation endmember values (uncertainty reported above), and the temperature-  
297  $\delta^2\text{H}_{\text{precipitation}}$  relationship and associated uncertainty reported below. Monte Carlo  
298 simulations were performed using 1000 iterations. To assess temperature changes  
299 between discrete time slices, we performed two-tailed Student's t-tests on the Monte  
300 Carlo distributions after compositing results for each time point within the periods of  
301 interest.

302

## 303 2.4 Climate Model Simulations

304 We use the Community Climate System Model 3 (CCSM3) global circulation  
305 model to test the effect of Bering Strait opening/closure and other glacial/interglacial  
306 boundary conditions on Beringian temperature and on Beringian sensitivity to global  
307 freshwater forcing events. The model has fully coupled atmosphere, land, ocean, and sea  
308 ice sub-models with a horizontal resolution of T42 or 2.8 degrees for atmospheric and  
309 land models and nominal 1 degree with enhanced meridional resolution to 1/3 degree in  
310 the equatorial tropics for the ocean and sea ice models. Boundary conditions are provided  
311 by Hu et al. (2015) and include changes to the Laurentide Ice Sheet, orbital forcing, and  
312 atmospheric greenhouse gas concentrations. Surface temperatures were averaged over  
313 100 years under 15 ka boundary conditions with an open and closed Bering Strait, and  
314 under present-day (1990 A.D.) boundary conditions with an open and closed Bering  
315 Strait. The model scenarios are idealized and not meant to represent the exact conditions  
316 under which the Bering Strait was flooded. Additionally, the same model configurations

are used to test the effect of freshwater addition to the North Atlantic on Beringian climate. Under the four scenarios described above (15 ka open/closed, 0 ka open/close), freshwater was gradually added to the North Atlantic until the AMOC collapsed, at which point surface temperatures from Beringia for the succeeding 100 years were averaged.

### 3 Results

#### 3.1 Modern Precipitation Isotopes

A total of 254 precipitation events at the Toolik Field Station were collected and analyzed, documenting a significant relationship between air temperature and  $\delta^2\text{H}$  (Figure 3). From this same dataset, Klein et al. (2015) use the  $\delta^{18}\text{O}$ -temperature regression,  $\delta^{18}\text{O} = 0.354 T - 21.11$ , to reconstruct temperatures at the McCall glacier over the past 70 years. For  $\delta^2\text{H}$ , the total least square regression has a slope of  $0.292 \text{ } \text{‰} \text{ } ^\circ\text{C}^{-1}$ , equivalent to  $3.4 \text{ } ^\circ\text{C } \text{‰}^{-1}$ . This value is in close agreement with the slope observed in other parts of Arctic North America (Porter et al., 2016). The root mean square error of the calibration is quite high at  $7.9 \text{ } ^\circ\text{C}$ , similar to the RMSE based on the  $\delta^{18}\text{O}$ , which is  $7.2 \text{ } ^\circ\text{C}$ .

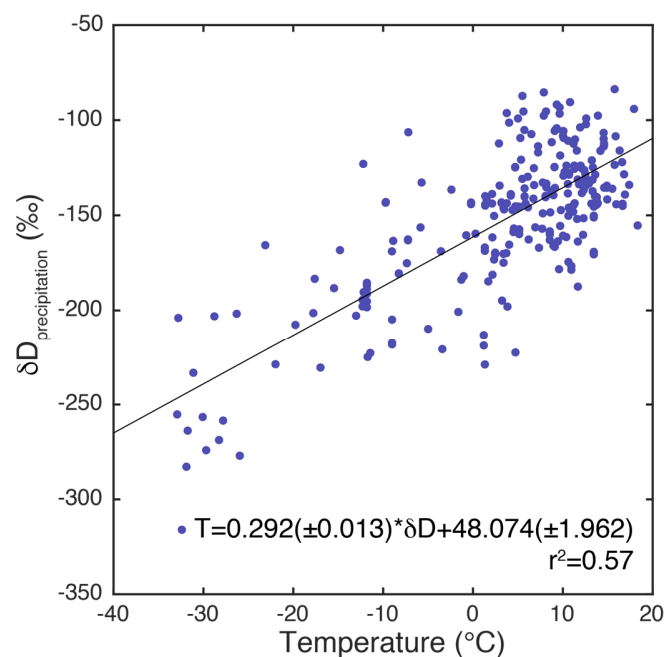


**Figure 3.** Modern relationship between  $\delta^2\text{H}_{\text{precipitation}}$  and air temperature at Toolik Lake, AK based on 254 precipitation events, supported in part by USNIP (US Network for Isotopes in Precipitation (Welker, 2000; Welker, 2012).

#### 3.2 Core chronology and lithology

338 Figure S2 shows the composite profile of overlapping core sections tied with  
339 distinct marker beds. The total core recovery was 500 cm, although there is significant  
340 distortion of bedding plains in the basal sections and so we only consider 480 cm of core  
341 in the composite here (Figure 2). The lowest radiocarbon sample dates to  $28,488 \pm 1001$   
342 ( $1\sigma$ ) calendar years before present, and extrapolation of the lower sedimentation rate  
343 produces a basal date of  $32,086 \pm 2197$  ( $2\sigma$ ) cal. yr BP. The 95% confidence interval  
344 ranges from  $\pm 4$  years at the core top to  $\pm 2208$  years at the base, and averages  $\pm 810$  years  
345 throughout the entire record. The age model is less-tightly constrained within the last  
346 glacial period.

347 Glacial-interglacial changes are evident in the MS, total organic carbon (TOC),  
348 and lithology profiles (Figure 2), and give rise to 3 distinct units that broadly correspond  
349 to the LGM, the last deglacial period, and the Holocene. The lower part of the core is  
350 characterized by low total organic carbon (TOC) (Vachula et al., 2019), averaging 4.9%,  
351 and magnetic susceptibility ranging from 0.5 to 46. A transition zone is apparent from  
352 205 to 103 cm, wherein TOC increases from less than 1% to 8-12%, and MS decreases.  
353 Above this transition zone physical properties are more stable, although TOC generally  
354 decreases upwards. Sediments consist of laminated, light brown, clay- to fine sand-sized  
355 material in the lower sections, laminated, black, silt from 205 to 103 cm, and massive,  
356 brown, silt from 103 cm to the coretop.

357 There is a series of sedimentary beds comprised of distinct gray clay (205-213  
358 cm, 235-237 cm, 258.5-264 cm, 266-268 cm, 271-273.5 cm, 285-288 cm, 289.5-295.5  
359 cm, 325-326 cm, 330-332 cm, 332.5-333 cm). Based on the sharp contact boundary with  
360 underlying sediments, these clay beds are interpreted as instantaneous depositional  
361 events. Sediment cores from Lake NE14, approximately 10 km from Lake E5, reveal a  
362 series of similar sedimentary units characterized by high clay content and a distinct  
363 geochemical signature (Chipman et al., 2016). The occurrence of these units in NE14 is  
364 linked to shoreline thermo-erosion events during exceptionally warm or wet summers. In  
365 Lake E5, radiocarbon ages of macrofossils from two of these layers are approximately  
366 35,000  $^{14}\text{C}$  yr bp (Figure 2), suggesting they contain aged terrestrial fragments and are  
367 likewise derived from periglacial erosion events along the shoreline.

368

369 3.3 *n*-acid distributions,  $^2\text{H}/^1\text{H}$  ratios, and vegetation correction

370 Leaf wax *n*-acids are present throughout the Lake E5 core, with the sum of *n*-C<sub>16</sub>-  
371 C<sub>32</sub> ranging from an average of 59  $\mu\text{g g sed}^{-1}$  in the glacial-aged sediments to 1596  $\mu\text{g g}$   
372  $\text{sed}^{-1}$  in the Holocene sediments (Figure 4). The carbon preference index is fairly high,  
373 averaging  $5.8 \pm 2.2$ , indicating that the waxes are derived from “fresh” plants and have  
374 undergone relatively little degradation (Bray and Evans, 1961) – they are unlikely to be  
375 sourced from shales in the Brooks Range mountains. The average chain length averages  
376  $25.3 \pm 0.8$ , and is highest in the deglacial sediments (Figure 4). Higher average chain  
377 length values are associated with greater aridity in the Arctic (Andersson et al., 2011),  
378 although Keisling et al. (2017) suggest that ACL also varies in response to temperature  
379 and vegetation change at Lake El’gygytgyn in Arctic Russia. Recent assessments from  
380 arctic tundra document that there is no clear relationship between plant taxa and *n*-acid  
381 homologue distributions (Dion-Kirschner et al., 2020; O’Connor et al., 2020). Thus it  
382 remains difficult to elucidate what drove the change in *n*-acid ACL. We note the  
383 increased ACL corresponds to higher representation of graminoid taxa in the pollen  
384 spectra, and suggest that that ACL change reflects the plant community turnover during  
385 the deglacial period.

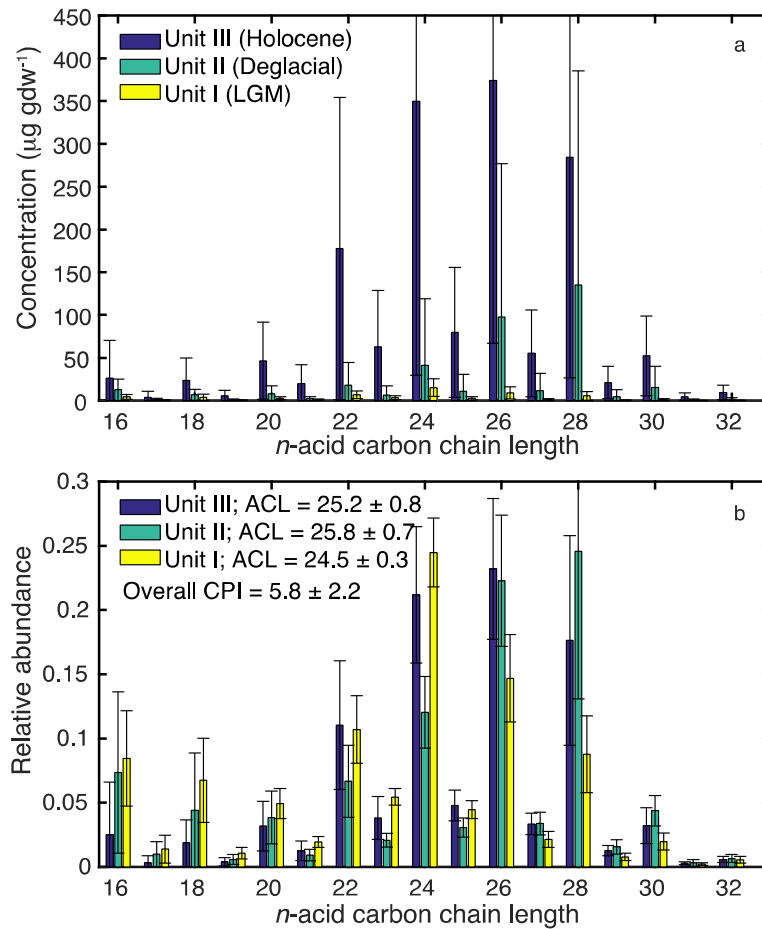


**Figure 4.** Leaf wax *n*-acid concentrations and distributions from Lake E5 sediments. Colors correspond to the three identified sedimentary units, which relate to the LGM (yellow), the last deglacial period (teal), and the Holocene (blue). a) *n*-acid concentrations s. b) Fractional abundance of *n*-acids relative to the C<sub>16</sub>-C<sub>32</sub> total. Error bars signify 1 standard deviation among samples of each unit.

The raw  $\delta^2\text{H}_{\text{wax}}$  values of C<sub>28</sub> and C<sub>26</sub> *n*-acids from Lake E5 are highly correlated ( $r^2=0.74$ , Figure S4), indicating that these compounds share common terrestrial sources. We focus on the C<sub>28</sub>  $\delta^2\text{H}_{\text{wax}}$ . Values range from -280 ‰ to -244 ‰ and the record exhibits distinct glacial-interglacial structure characterized by more negative values during the last glacial period, a peak in the early Holocene, and a declining trend thereafter until the last 150 years (Figure 5). The most pronounced change is a step-increase in  $\delta^2\text{H}_{\text{wax}}$  centered at  $11.6 \pm 0.2$  ka, coinciding with the termination of the Younger Dryas stadial. Other Alaska isotope records that span the YD interval, namely

401  $\delta^{18}\text{O}$  of ice wedges (Meyer et al., 2010) and  $\delta^{18}\text{O}$  of willow stems (Epstein, 1995;  
402 Gaglioti et al., 2017) also show a rapid increase at the termination of the YD (Figure 6).  
403 In these records, pre-YD  $\delta^{18}\text{O}$  values are comparable to the post-YD values, suggesting  
404 the YD was a brief interruption between Bølling and early Holocene warmth as is evident  
405 in Greenland ice core  $\delta^{18}\text{O}$  (Buizert et al., 2014). In contrast,  $\delta^2\text{H}_{\text{wax}}$  values of the Bølling  
406 warm period do not achieve post-YD values at Lake E5 and are only slightly  $^2\text{H}$ -enriched  
407 relative to LGM samples. One possibility for this contrast is if the water isotope proxies  
408 record different seasons and the Bølling-Allerød temperature change was more  
409 pronounced in winter than summer as it was in the North Atlantic region (Atkinson et al.,  
410 1987; Denton et al., 2005). Given that the willow stems analyzed by Gaglioti et al. (2017)  
411 are thought to capture the same seasonality as the leaf waxes, however, it is more likely  
412 that a temporary expansion of graminoid sedges during the Bølling-Allerød and late  
413 deglacial (Eisner and Colinvaux, 1992; Abbott et al., 2010) impacted the record of  
414  $\delta^2\text{H}_{\text{wax}}$ , masking a potential BA signal. A slight shift toward longer carbon chain lengths  
415 in the  $n$ -acid distributions in the deglacial sediments is evidence for a potential vegetation  
416 effect on the leaf waxes. Because Arctic graminoids express stronger  $^2\text{H}/^1\text{H}$  fractionation  
417 than dicotyledenous shrubs or forbs (Daniels et al., 2017; Daniels et al., 2018; Berke et  
418 al., 2019), the observed vegetation change would suppress a change in  $\delta^2\text{H}_{\text{wax}}$  during the  
419 Bølling interval.



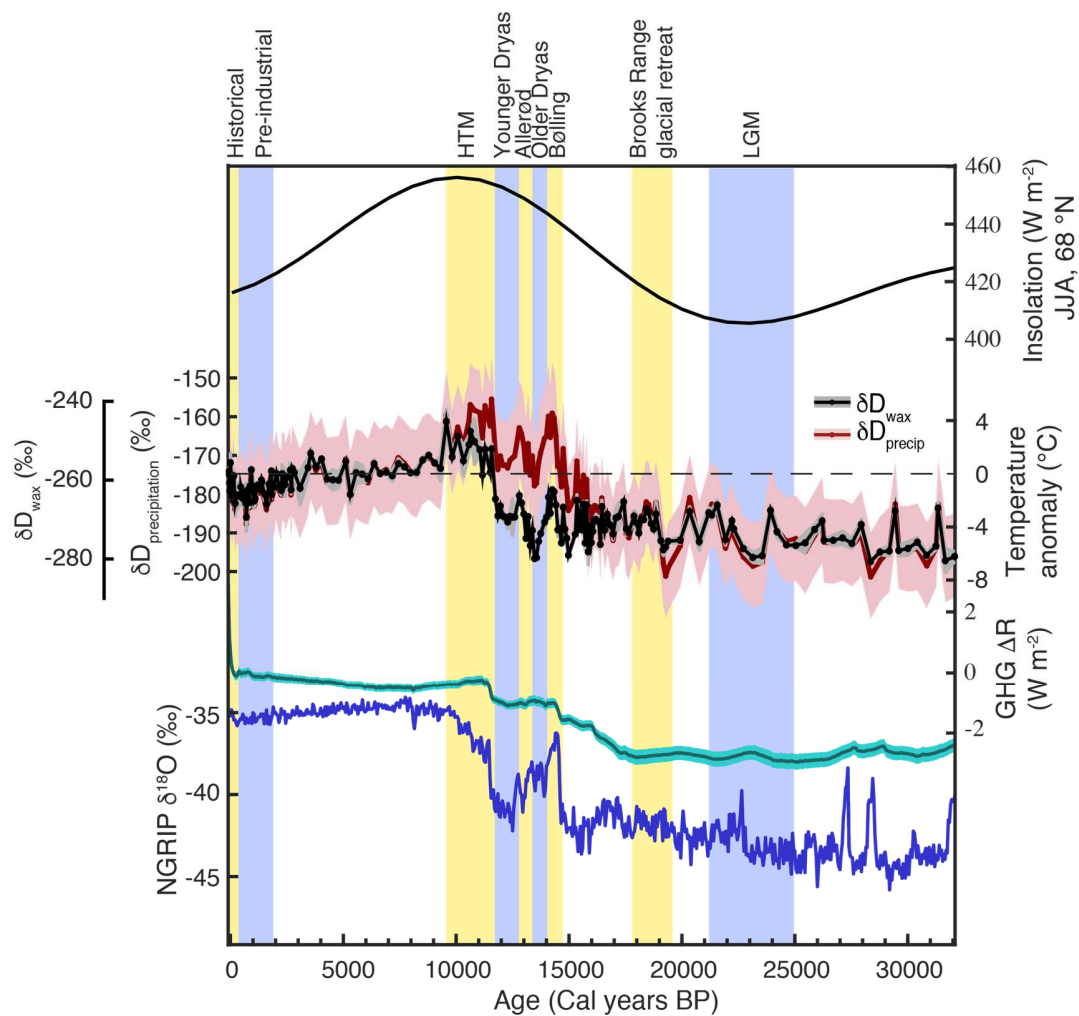


**Figure 5.** A comparison between summer (JJA) insolation (Laskar et al., 2004), Lake E5  $\delta^2\text{H}_{\text{wax}}$  (black) and inferred  $\delta^2\text{H}_{\text{precipitation}}$  and temperature anomalies with 75% and 25% confidence bounds shown for temperature estimates (red with pink shading), relative greenhouse gas radiative forcing from  $\text{CO}_2$ ,  $\text{CH}_4$ , and  $\text{N}_2\text{O}$  (Köhler et al., 2017), and the NGRIP  $\delta^{18}\text{O}$  record (Andersen et al., 2004).

The effect of the vegetation-based correction (Figure S3) is most notable during the deglacial period, and brings the Bølling- to post-YD differential in better alignment with the Alaska  $\delta^{18}\text{O}$  records (Figure 6). It also slightly amplifies glacial-interglacial  $\delta^2\text{H}$  change, as there were more graminoids during the glacial period than the Holocene, and also indicates that changes in  $\delta^2\text{H}_{\text{precipitation}}$  likely began prior to the 11.6 ka step change.

The propagation of analytical and calibration uncertainty results in fairly large uncertainty for the calculated  $\delta^2\text{H}_{\text{precipitation}}$  and temperature reconstruction values.

Analytical uncertainty of  $\delta^2\text{H}$  measurements is excellent, with a pooled standard

deviation of replicate measurements of 1.4 ‰ (Table S3). After consideration of the changing vegetation assemblages and the assumed end member fractionation values and their uncertainty, the 95% confidence interval on the reconstructed  $\delta^2\text{H}_{\text{precipitation}}$  measurements is  $\pm 22$  ‰, similar to the root square error for *n*-acids and *n*-alkanes conversions globally (McFarlin et al., 2019). This level uncertainty is on the same order of magnitude as the observed changes in  $\delta^2\text{H}_{\text{wax}}$  over the Lake E5 record. The 25%-75% CI for  $\delta^2\text{H}_{\text{precipitation}}$  is  $\pm 9$  ‰ and is shown in the figures. After converting these values to temperature and assessing the anomaly from present day, we find that the temperature change has a 95% confidence interval of  $\pm 8^\circ\text{C}$ . The 25-75% CI for temperature is  $\pm 3.5^\circ\text{C}$ .

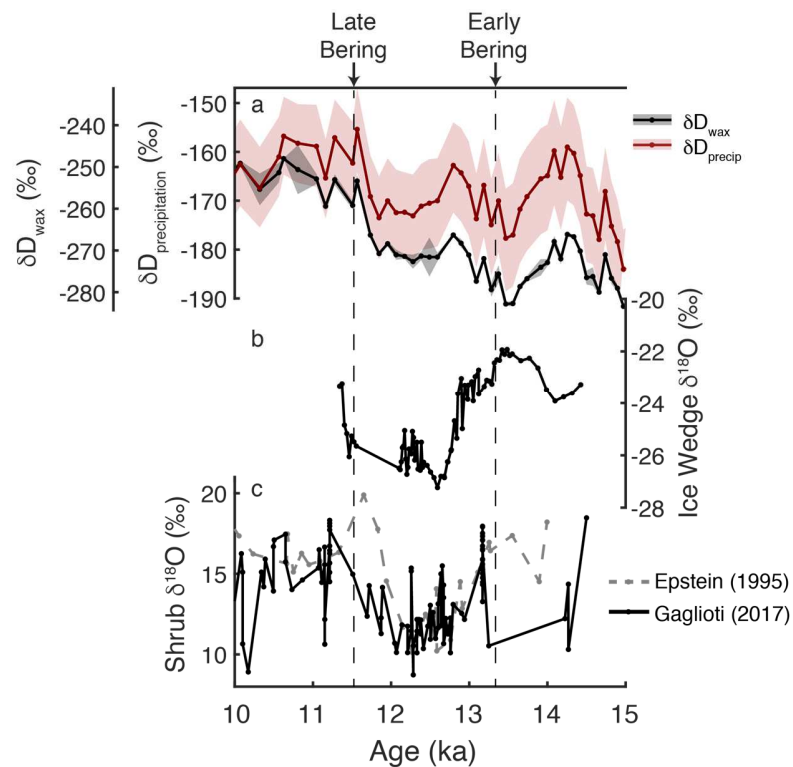


**Figure 6.** Comparison of Alaska water isotope records during the Younger Dryas interval demonstrating that the vegetation-based correction brings the Lake E5 D/H record into better agreement with other nearby isotope records. a) Ice-volume corrected  $\delta^2\text{H}_{\text{wax}}$  from Lake E5 (black with gray shading showing 1σ of analytical uncertainty), and the inferred  $\delta^2\text{H}_{\text{precipitation}}$  following application of the pollen-guided fractionation factors (red with pink shading showing 25 and 75% confidence intervals of the monte carlo simulation); b) Ice wedge  $\delta^{18}\text{O}$  values from Barrow, Alaska (Meyer et al., 2010); c) Salix (willow shrub) cellulose  $\delta^{18}\text{O}$  from the North Slope of Alaska (Epstein, 1995; Gaglioti et al., 2017). Timing of the dual-phase opening of the Bering Strait is also shown (Pico et al., 2020).

456

## 457 **4. Discussion**

### 458 4.1 Climatic interpretation of $\delta^2\text{H}_{\text{precipitation}}$

459         Due to the strong relationship between air temperature and  $\delta^2\text{H}_{\text{precipitation}}$  in the  
460 Arctic (Dansgaard, 1964) and at the Toolik Field Station (Figure 3),  $\delta^2\text{H}_{\text{precipitation}}$  is a  
461 useful proxy for reconstructing past air temperature (Pautler et al., 2014; Klein et al.,  
462 2015; Porter et al., 2019). Changes in moisture source that resulted from changes in  
463 Arctic sea ice cover, site continentality, or prevailing wind directions could impart effects  
464 on  $\delta^2\text{H}_{\text{precipitation}}$  at Lake E5, but we posit that such effects are secondary to the control of  
465 condensation temperature at the site, and that they in fact contribute to the empirical  
466 relationship between temperature and  $\delta^2\text{H}_{\text{precipitation}}$  that we observe in modern monitoring.  
467 The Arctic Ocean, Bering Sea, and North Pacific are the dominant sources of moisture to  
468 the North Slope of Alaska (Mellat et al., Submitted). Precipitation originating in the Gulf  
469 of Alaska is more  $^2\text{H}$ -depleted than Arctic Ocean or Bering Sea moisture sources because  
470 of a larger rainout trajectory and orographic rainout as airmasses move across the Alaska  
471 interior (Lachniet et al., 2016; Putman et al., 2017; Bailey et al., 2019). The more  
472 negative  $\delta^2\text{H}$  signature of southern airmasses occurs despite the Arctic Ocean being  
473  $\sim 15\text{‰}$   $^2\text{H}$ -depleted relative to the North Pacific (Schmidt et al., 1999). A smaller-scale  
474 and reversed precipitation isotope gradient is also observed across the North Slope,  
475 wherein Arctic Ocean-sourced moisture becomes  $^2\text{H}$ -depleted as it travels southeastward  
476 (Gaglioti et al., 2017). Although these “source effects” are influential, seasonal changes  
477 in moisture source are largely controlled by sea ice coverage, which together with air  
478 temperature, gives rise to a strong seasonal cycle in  $\delta^2\text{H}_{\text{precipitation}}$  at Lake E5 (Daniels et  
479 al., 2017) and a positive correlation between air temperature and  $\delta^2\text{H}_{\text{precipitation}}$  (Figure 3).  
480 Because these seasonal changes are analogous to changes over glacial-interglacial time  
481 scales, the modern temperature- $\delta^2\text{H}_{\text{precipitation}}$  relationship offers a transfer function for  
482 approximating past temperature in northern Alaska.

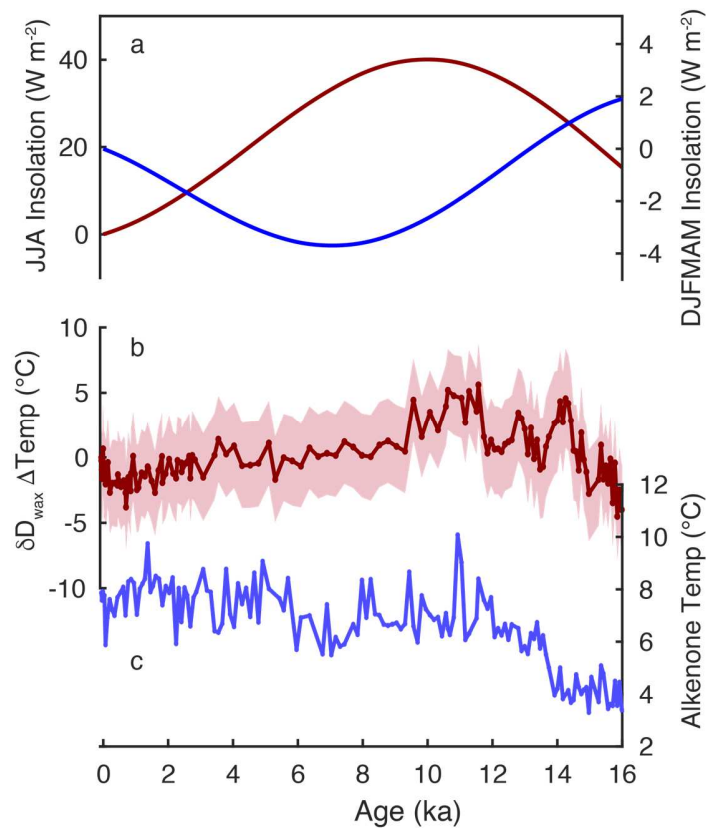
483         The utility of the modern temperature- $\delta^2\text{H}_{\text{precipitation}}$  relationship is further  
484 supported by an investigation of isotope-enabled climate model simulations of the past 20  
485 ka which shows that the relationship between temperature and  $\delta^2\text{H}_{\text{precipitation}}$  has remained  
486 approximately constant since the LGM (Figure S5). The modeled modern slope is

substantially lower than the observed relationship between temperature and  $\delta D_{\text{precipitation}}$ , but the modeled slopes remains stable during and since the LGM, reflecting the approximate stationarity of the temperature- $\delta^2 H_{\text{precipitation}}$  relationship over this interval and adding confidence in the temperature interpretation of the  $\delta^2 H_{\text{precipitation}}$  record. Temperature anomalies are calculated using the observed modern slope of  $3.4 \text{ ‰ } ^\circ\text{C}^{-1}$ , which is similar to the slope reported across a number of Arctic North American sites ( $3.1 \text{ ‰ per } ^\circ\text{C}$  Porter et al., 2016).

Estimates of temperature change from  $\delta^2 H_{\text{wax}}$  are also influenced by the seasonality of precipitation used for plant leaf wax synthesis. Although tundra plant growth is constrained to the summer growing season, the water used in their biosynthesis has been linked to both warm and cold season precipitation sources (Welker et al., 2005; Jespersen et al., 2018). Wilkie et al. (2012) suggest a bias toward use of remnant autumnal precipitation in supporting spring leaf production, whereas others have used terrestrial wax  $^2\text{H}/^1\text{H}$  as a proxy for summer precipitation (Thomas et al., 2012; Porter et al., 2016). In our study area, approximately 60% of the annual precipitation falls during JJA (Cherry et al., 2014); Daniels et al. (2017) identify seasonally changing soilwater isotopic composition throughout the growing season and suggest that although cold season precipitation can contribute to biosynthesis, summer rainfall is the most important hydrogen source for leaf wax production. Given the mixture of seasonal precipitation utilized by tundra plants, the potential for changing growing season lengths, and the strong event-based correlation between temperature and  $\delta^2 H_{\text{precipitation}}$  across the seasons, we use the annual temperature- $\delta^2 H_{\text{precipitation}}$  relationship to translate our  $\delta^2 H_{\text{wax}}$  measurements into summer-biased temperature change estimates.

The seasonal nature of the leaf wax proxy is exemplified in a direct comparison with the lacustrine alkenone record from Lake E5 (Figure 5; Longo et al., 2020). Alkenone production was observed to be greatest early in the spring in Arctic lakes (Longo et al., 2016), and as such, the alkenone-inferred temperatures are sensitive to spring ice cover and cold-season conditions. During the deglacial period, both alkenone and  $\delta^2 H_{\text{wax}}$  suggest warming of a similar magnitude, albeit with some differences in the timing and the nature of abrupt climate events. Both proxies exhibit an early temperature maximum in the early Holocene, after which they diverge substantially, with alkenones

518 showing a general warming trend, particularly in the last 8 kyr, whereas  $\delta^2\text{H}_{\text{wax}}$  showing a  
 519 cooling trend over the same interval. This contrast signifies that the temperatures of  
 520 different seasons are responding to different drivers over the Holocene. Namely, cold-  
 521 season temperatures appear to be sensitive to winter insolation and greenhouse gas  
 522 forcing (Longo et al., 2020), while summer temperatures show a stronger relationship  
 523 with summer insolation.



524  
 525 **Figure 7.** Comparison of Lake E5 alkenone- and  $\delta^2\text{H}_{\text{wax}}$ -inferred temperature changes. a)  
 526 Deviations from present day in mean insolation at 68  $^{\circ}\text{N}$  for summer (JJA, red) and the  
 527 cold season (DJFMAM, blue). b) Temperature anomaly based on the leaf wax  $^2\text{H}/^1\text{H}$   
 528 proxy, with 25% and 75% confidence interval. c) Alkenone-derived temperatures (Longo  
 529 et al., 2020).  
 530

## 531 4.2 Glacial-Interglacial Climate Change

532 The vegetation-corrected  $\delta^2\text{H}_{\text{precipitation}}$  and inferred temperatures at Lake E5  
 533 exhibit distinct glacial-interglacial structure (Figure 6), with LGM  $\delta^2\text{H}_{\text{wax}}$  approximately  
 534 10-15 ‰ more negative than today. This magnitude of change is similar to that observed  
 535 in leaf waxes in the Yukon Territory (Pautler et al., 2014). Based on the Monte Carlo

simulations, inferred temperatures during the LGM were approximately 4 °C lower than during the Historical Period (1900-2014 CE), with iterations ranging from 10 °C cooler to 2 °C warmer. Compared to the Pre-industrial period (PI; 2-0.1 ka), LGM temperatures were just 3 °C cooler (Monte Carlo range: -8 to +3 °C). The estimated  $\Delta T$  of 4°C for the LGM is less severe than LGM cooling observed in Greenland, northern Europe, and other parts of North America (Figure 8), but is within the range of previous estimates for Eastern Beringia (Table S4, and references therein). For Beringia, 18 warm-season temperature reconstructions have an average LGM temperature change of -4°C. The six sites fringing the Laurentide Ice Sheet, combined with Greenland borehole temperature, had an average temperature change of -18 °C. Asia and Europe saw  $\Delta T$  of -3 and -6 °C, respectively. We examined the ensemble output from the Paleoclimate-Model Intercomparison Project 3 (PMIP3) and find that the model results generally agree well with proxy reconstructions (Figure 8), simulating strongest cooling around the Laurentide and Greenland Ice Sheets and relatively weak cooling over Beringia. The model slightly overestimates cooling in mid- to high-latitude Europe. Additional proxy reconstructions from Asia are needed to evaluate the spatial pattern of LGM temperature change there. The mild conditions reconstructed for Beringia may have been important for maintaining the highly-productive mammoth-steppe tundra (Zimov et al., 2012) and sustaining human occupation of Beringia through the LGM (Goebel et al., 2008; Vachula et al., 2019).

Our finding of relatively weak summertime cooling during the LGM could support the hypothesis that the orographic effect of the Laurentide Ice Sheet was to steer relatively warm air into the region (Otto-Bliesner et al., 2006; Briner and Kaufman, 2008; Bartlein et al., 2011). Other mechanisms may have also contributed to maintaining the mild summer climate. For example, Löffverström and Liakka (2016) suggest that reduced cloud cover during the LGM allowed more downwelling shortwave radiation to reach the land surface, further contributing to warmth in Alaska, an effect that would be most impactful during summer. Using a compilation of sea surface temperatures, Rae et al. (2020) show that the North Pacific surface ocean was 2 °C warmer during the LGM than at present, owing to strengthened meridional heat transport in the Pacific. This oceanic warming may have had regional impacts on surface temperature. Furthermore, in the CCSM3 simulations (Figure 8), mild LGM temperatures are localized over the Bering

567 Strait, implying that exposure of the Bering Land Bridge, through its effects on surface  
568 energy balance (Bartlein et al., 2015), may have partially offset LGM summertime  
569 cooling in the immediate Bering Strait vicinity. West of the Bering Strait, moderating  
570 effects of the ice-sheet orography and land-bridge were less pronounced, with LGM  
571 summer temperatures at Lake El'gygytgyn in Far East Russia 8-9 °C colder than present  
572 (Melles et al., 2012), nearly double the global average of 4.9 °C (Shakun and Carlson,  
573 2010). Thus, while much of North America, Europe, and Asia experienced enhanced  
574 LGM cooling due to continental ice sheet and sea ice growth and possible redirection of  
575 polar air masses into those regions (Miller et al., 2010), Beringia-specific changes in land  
576 exposure and the advection of relatively warm air dampened LGM cooling, resulting in  
577 regionally distinct expressions of Arctic Amplification.

578         There are few records of winter LGM climate with which to compare the summer  
579 reconstructions. Pollen-based inferences suggest comparable magnitude of winter and  
580 summer temperature change in Alaska (Viau et al., 2008), although these authors note  
581 that deconvolving seasonal signals from pollen is tenuous in the region. To the southeast  
582 of our site, in central Yukon Territory and in close proximity to the Laurentide and  
583 Cordilleran Ice Sheets, Pautler et al. (2014) analyzed multiple biomarkers and found that  
584 the winter-biased proxy showed a greater LGM temperature change than the warm-season  
585 proxy. Porter et al. (2016) report that annual and cold-season temperatures of the Yukon  
586 were ~14-21 °C below present day but did not independently constrain warm season  
587 temperatures. In Siberia, pollen spectra suggest that LGM cooling was approximately  
588 twice as strong in winter as summer (Wetterich et al., 2011). Likewise there is a strong  
589 seasonal difference in LGM climate change in the North Atlantic (Denton et al., 2005), in  
590 large part because the sea ice feedbacks are stronger in winter than in summer. As  
591 mentioned previously, ice wedges and lacustrine alkenones are two approaches to  
592 investigate past winter conditions in Beringia. Currently, records of these proxies are  
593 found from the late glacial through the Holocene (Meyer et al., 2010; Longo et al., 2020),  
594 and reconstructions extending through the LGM may help decipher how summer and  
595 winter climate drivers differed.

596  
597

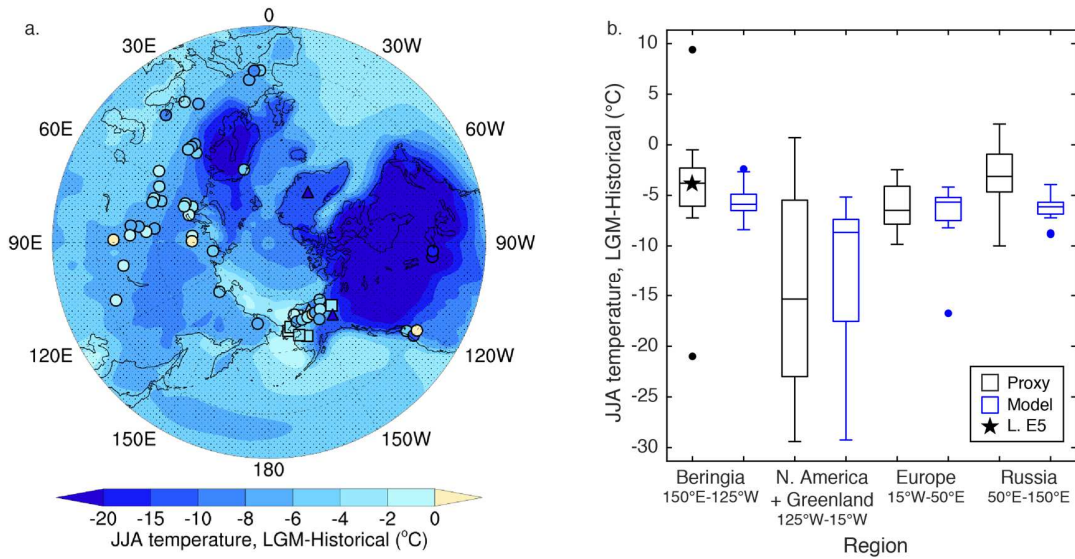


**Figure 8.** Data-model comparison of LGM warm-season temperature anomalies across the Arctic. **a.** PMIP3 multi-model ensemble average JJA temperature anomalies relative to the historical period (1900-2000 CE) overlain by published LGM temperature reconstructions based on pollen (circles), insects (squares), and geochemistry (triangles) (Table S4). **b.** LGM temperature anomalies in proxies and the multi-model means in four sectors of the Arctic. Model data are extracted from gridcells within 2° of proxy sites, and do not include ice-sheet or ocean cells, with the exceptions of the Greenland and Norway locations, for which ice-free grid cells are not available in models.

#### 4.3 Rapid Changes During the Glacial Termination

$\delta^2\text{H}_{\text{precipitation}}$  at Lake E5 generally tracks changes in summer insolation. Increasing  $\delta^2\text{H}_{\text{precipitation}}$  is evident as early as  $23.1 \pm 0.9$  ka, and steady, more substantial increase began at  $16.9 \pm 0.5$  ka, coinciding with increased radiative forcing from greenhouse gases (Köhler et al., 2017), and culminating in a brief periods of rapid rise at  $14.8 \pm 0.3$  ka and again at  $11.6 \pm 0.2$  ka. Inferred temperatures rose by  $\sim 8$  °C (Monte Carlo range: +6 to +10 °C) from the LGM to an early Holocene thermal maximum (HTM) from 11.6-9.5 ka, then cooled steadily until the PI era. While the overall correspondences between temperature, greenhouse gas forcing, and summer insolation are strong, we observe several intervals of abrupt warming and cooling during the glacial termination (Figure 5).

Early in the glacial termination, there was rapid  $\delta^2\text{H}_{\text{wax}}$  increase from  $19.3 \pm 0.7$  ka to  $18.9 \pm 0.7$  ka. The magnitude is estimated to be equivalent to  $\sim 4$  °C (Monte Carlo range: +0 to +8 °C). The warming can help explain suggestions of rapid glacier retreat in the nearby Brooks Range mountains dated to 19 ka (Pendleton et al., 2015). The causes



for this early, strong warming have been enigmatic, and include increasing summer insolation and a maximum in the effect of the LIS on atmospheric flow (Pendleton et al., 2015), but it is unclear how these processes would produce the abrupt, short-lived warming observed in the  $\delta^2\text{H}_{\text{wax}}$  record. We propose an oceanic driver of this warming event. Ventilation ages of the North Pacific document an invigorated PMOC beginning at 19 ka (Figure 9) which would have increased the total northward heat transport in the Pacific by approximately 0.7 PW, with the greatest amount of resultant ocean warming near the Gulf of Alaska and Bering Strait (Okazaki et al., 2010). Model simulations indicate that PMOC intensifies in response to AMOC collapse (Hu et al., 2012), for example during HS1, due to reduced evaporation and increased sea surface salinity in the North Pacific. We note, however, that empirical evidence for PMOC intensification predates the reduction in AMOC marking the onset of HS1 (Figure 6; McManus et al., 2004; Okazaki et al., 2010). While the cause of the potential PMOC invigoration remains uncertain, the increased northward oceanic heat transport in both oceans just prior to HS1 likely contributed to warming from 19-18 ka in Alaska, while subsequent HS1 cooling may have been suppressed in Alaska by sustained PMOC activity.

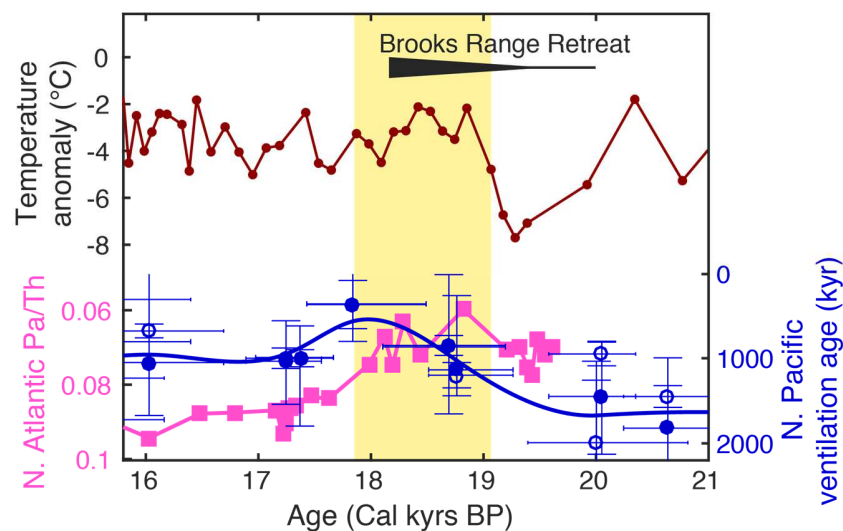


**Figure 9.** Comparison of early deglacial warming at Lake E5 and marine indicators of PMOC and AMOC intensity. Lake E5 temperature anomaly (red) is based on  $\delta^2\text{H}_{\text{wax}}$  relative to the historical period. N. Pacific ventilation ages (blue) reflect PMOC intensity (Okazaki et al., 2010), while Pa/Th from the Bermuda Rise (magenta) is an indicator of AMOC intensity (McManus et al., 2004). Also shown is the period of rapid glacier retreat in the Brooks Range mountains near Lake E5 (Pendleton et al., 2015).

646 Abrupt  $\delta^2\text{H}_{\text{wax}}$  increases at  $14.8 \pm 0.3$  and  $11.6 \pm 0.2$  ka in the Lake E5 record  
 647 (Figure 5 and 3) correspond with the onset of the Bølling interstadial and the termination  
 648 of the Younger Dryas, indicating Arctic Alaskan temperature change was positively  
 649 correlated with changes in the North Atlantic during the latter part of the deglaciation.  
 650 Reconstructed temperature change was approximately +4 °C (Monte Carlo range: +1 to  
 651 +8 °C) at the Bølling onset and +3 °C (Monte Carlo range: -4 to +8 °C) over the YD  
 652 termination, much smaller than the 9 °C changes reconstructed over Greenland  
 653 (Severinghaus and Brook, 1999). Both events are driven by strengthening and possible  
 654 “overshoot” of AMOC (Liu et al., 2009). While BA-YD fluctuations are seen in  
 655 oceanographic records of the Bering Sea (Kühn et al., 2014) and Gulf of Alaska  
 656 (Praetorius and Mix, 2014), the much larger surface warming observed at Greenland  
 657 indicates that the surface temperature response to AMOC variability is weaker in  
 658 continental Beringia. Furthermore, comparison of the Lake E5  $\delta\text{D}_{\text{precipitation}}$ , which records  
 659 summer variability, with ice wedge isotopes in Barrow, AK, which record winter  
 660 conditions, suggests that the BA-YD oscillation impacted all seasons, but was expressed  
 661 most strongly in the winter season (Figure 6). Nevertheless, the two events encompass  
 662 most of the deglacial temperature increase at Lake E5. The Bølling-onset inferred here  
 663 coincides with expansion of graminoid sedges and precedes a vegetation shift from herb  
 664 steppe tundra to deciduous shrub tundra between 13.9 and 12.6 seen in Brooks Range-  
 665 area pollen records (Oswald et al., 1999; Mann et al., 2002; Abbott et al., 2010). We  
 666 speculate that the temporary expansion of sedges was in part responsive to increased  
 667 moisture availability during the BA, and subsequent warming towards the end of the YD  
 668 promoted the expansion of *Betula* and other shrubs (Figure S3). The expansion of shrubs  
 669 would have accelerated deglacial warming by increasing the surface energy balance of  
 670 the Alaska land surface by 2-3 W m<sup>-2</sup> (Lynch et al., 1999), similar to changes occurring  
 671 today (Sturm et al., 2001; Elmendorf et al., 2012). The relatively low-resolution sampling  
 672 of the pollen make it difficult to determine if the isotopic proxy and vegetation  
 673 assemblages have different response times to climate change.

674 The pre-YD warm interval occurred in two phases, interrupted by a short-lived  
 675 cool period at approximately 14 ka correlating with the Older Dryas interval recognized  
 676 from the North Atlantic (Grootes and Stuiver, 1997; Mangerud et al., 2017) region as

677 well as the North Pacific (Kienast and McKay, 2001). Following this,  $\delta^2\text{H}_{\text{wax}}$  increased,  
678 with inferred temperatures increasing by 3 °C (+1 to +4 °C) between  $13.5 \pm 0.3$  and  $12.8$   
679  $\pm 0.2$  ka, marking the onset of a warm interval correlating with the Allerød Interstadial. In  
680 contrast to the NGRIP isotope record which suggests cooling across the B-A (Andersen  
681 et al., 2004) the Bølling and Allerød periods are of comparable temperatures at Lake E5.  
682 This contrast is also recognized in Southern Alaska (Hu et al., 2006), and could arise  
683 from processes local to Beringia, such as the flooding of the Bering Land Bridge, which  
684 possibly enhanced Allerød warming in the area.

685         The submergence of the Bering land bridge during the late deglacial likely had  
686 profound impact on Beringia climate (Bartlein et al., 2015). The Pacific and Arctic  
687 Oceans became connected between 11 and 13.4 ka (Elias et al., 1996; Keigwin et al.,  
688 2006; England and Furze, 2008; Jakobsson et al., 2017), although the timing is not  
689 precisely known (Clark et al., 2014). Geophysical modeling of regional ice sheets and  
690 isostatic adjustment suggests the possibility of a two-phase land bridge inundation, with  
691 the first Pacific-Arctic connection forming ~13.3 ka, followed by a more substantive  
692 flooding event ~11.5 ka, with these periods bracketing an approximate intermission in  
693 local sea level change (Pico et al., 2020). Their model identifies regional isostatic  
694 rebound from 13 to 11.5 ka, driven by mass loss from the Cordilleran and western  
695 Laurentide Ice Sheet, as the principal driver of the hiatus in Bering Strait flooding. If the  
696 summer warming signal at 13.4 ka in the Lake E5  $\delta^2\text{H}_{\text{wax}}$  record represents the broader  
697 region, this may have provided an important mechanism contributing to retreat of the  
698 Cordillaran Ice Sheet or western Laurentide Ice Sheet at that time.

699         We tested the impacts of Bering submergence using idealized experiments in  
700 CCSM3 by simulating Beringia surface temperatures under Bering Strait open and closed  
701 scenarios (BSO and BSC) and under 15 ka (deglacial) and 0 ka (interglacial) climate  
702 boundary conditions. Upon opening of the strait we observe little change, or cooling in  
703 the annual temperature immediately over the Bering Sea. However, moving away from  
704 the strait, the effect is reversed, with 0.5-1.5 °C warming over interior Alaska (Figure  
705 10). The warming effect is stronger under interglacial climate conditions. Under late  
706 glacial boundary conditions, the warming impact of Bering submergence is strongest over  
707 southeast Alaska. Thus, although the simulations are idealized and do not test the climate

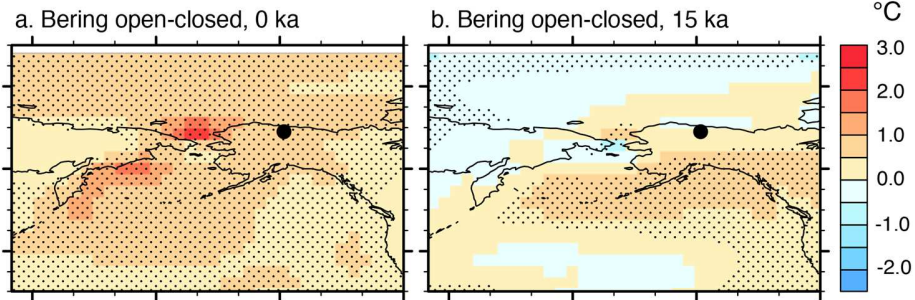
708 impacts of initial strait opening, they provide qualitative support for the idea that  
709 increased Bering Strait throughflow warms interior Alaska, despite the fact that the  
710 marine transgression resulted in summer cooling in the immediate vicinity of the Bering  
711 Strait. An early opening of the Bering Strait (~13.3 ka) may therefore be linked to the  
712 enhanced Allerød warming signal at Lake E5, whereas a late opening (~11.5 ka) may  
713 have contributed to YD-termination warmth and a sustained early Holocene warm period  
714 in Eastern Beringia.

715         Abrupt warming events at 13.5 ka and 11.6 ka bracket a Younger Dryas cool  
716 interval. Across Eastern Beringia, indications of YD climate anomalies variably are  
717 absent (Kokorowski et al., 2008; Kurek et al., 2009a; Kurek et al., 2009b), demonstrate  
718 wintertime cooling (Meyer et al., 2010), demonstrate summertime cooling (Engstrom et  
719 al., 1990; Hamilton, 2003; Mann et al., 2010; Gaglioti et al., 2017), or suggest a return to  
720 arid conditions (Abbott et al., 2000; Mann et al., 2002). In Lake E5,  $\delta^2\text{H}_{\text{wax}}$  decreased by  
721 10 ‰ beginning at  $12.8 \pm 0.2$  ka, equivalent to approximately 3 °C of summer cooling.

722         The YD climate reversal is typically attributed to surface water freshening in the  
723 North Atlantic, slowing of AMOC, and reduction of northward oceanic heat transport  
724 into the high northern latitudes. We tested the impacts of these processes on Beringian  
725 climate using idealized freshwater hosing experiments in the CCSM3 by simulating  
726 AMOC collapse under the same scenarios as the Bering Strait experiments (Figure 10).  
727 Under deglacial boundary conditions, AMOC collapse results in a range of cooling of 1-3  
728 °C in Alaska for a fully-open strait and 0-2 °C when the strait is still closed. Under  
729 present-day (0 ka) boundary conditions, the temperature sensitivity to North Atlantic  
730 freshwater forcing is approximately double that of the deglacial simulations for both BSO  
731 and BSC scenarios, suggesting that a weakened AMOC has a much larger impact on  
732 Arctic Alaskan climate when the global climate is warmer. In addition, the prediction that  
733 the magnitude of cooling is ~50% weaker when the Bering Strait is closed, may help  
734 explain the weak expression of HS1 in Lake E5 sediments.

735

### Bering Strait Experiments



### Bering Strait x Hosing Experiments

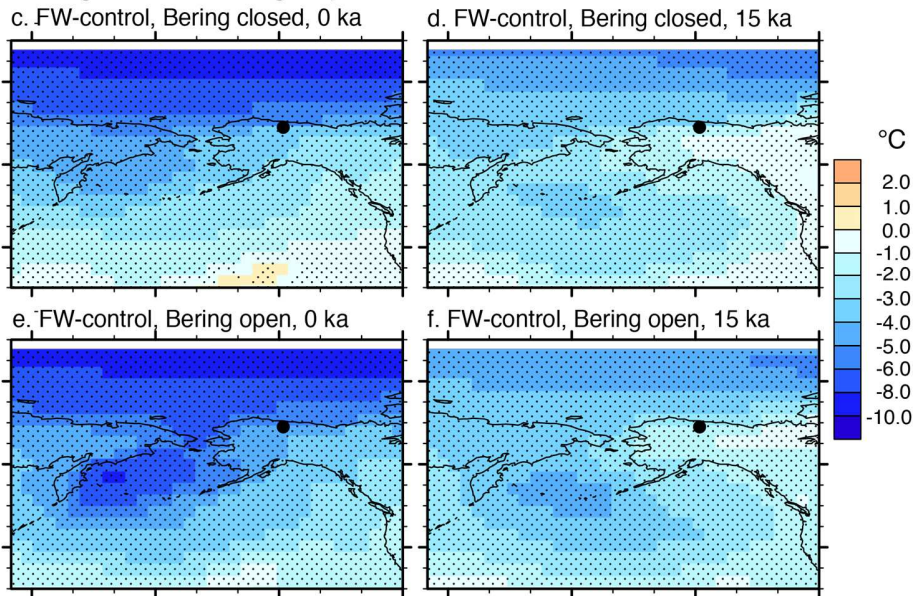


**Figure 10:** Mean annual surface temperature anomalies in Beringia in CCSM3 experiments. Stippling represents anomalies that are statistically significant at the  $p = 0.05$  level according to a t-test. **a.** and **b.** Mean annual temperature anomalies between simulations with open and closed Bering Strait under present-day (1990 A.D.) and 15 ka boundary conditions, respectively; **c.** and **d.** Mean annual temperature anomaly between hosing experiments and control simulations under closed Bering Strait conditions for 0 ka and 15 ka; **e.** and **f.** Same as **c.** and **d.** but with an open Bering Strait.

### 3.4 Climate of the Holocene

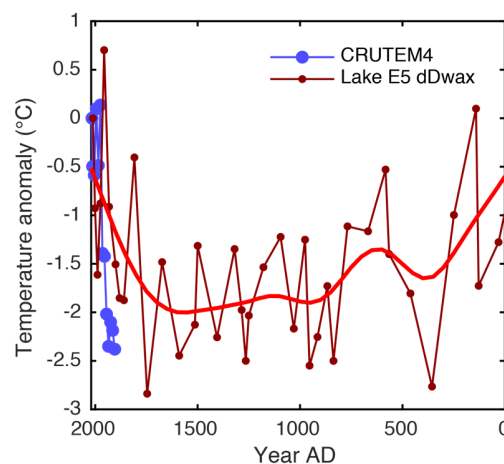
The most prominent feature of the Holocene is a  $\delta^2\text{H}_{\text{precipitation}}$  and inferred-temperature maximum from ~11.6 to 9.5 ka (Figure 5), followed by a gradual cooling until the PI period. The inferred  $\delta^2\text{H}_{\text{precipitation}}$  was 19 ‰ higher during this early Holocene Thermal Maximum (HTM) compared to PI period, while temperatures averaged 6 °C warmer (Monte Carlo range: +0 to +10 °C). Compared to the Historical period,  $\delta^2\text{H}_{\text{precipitation}}$  during the HTM was 16‰ higher and temperatures averaged 4 °C warmer

752 (Monte Carlo range: -1 to +10 °C). The timing of the HTM is approximately synchronous  
753 with peak NH summer insolation (Figure 5), and occurs slightly earlier than in the Yukon  
754 Territory (Porter et al., 2019) and locations further east (Kaufman, 2004). The  
755 termination of the HTM occurs abruptly, with ~2 °C of cooling at  $9.5 \pm 0.2$  ka, followed  
756 by gradual cooling that follows trends in summer insolation.

757         While most records from the region agree that early Holocene temperatures were  
758 as warm or warmer than present, the inferred magnitude Holocene cooling at Lake E5  
759 exceeds some but not all estimates for Alaska. Summer temperatures along the Chukchi  
760 Sea coastal region were 4-6 °C warmer than present, based on fossil beetle assemblages  
761 (Elias et al., 1996), in good agreement with the  $\delta D_{wax}$  inference. Lacustrine chironomid  
762 records from Zagoskin Lake near the Bering Strait (Kurek et al., 2009a) and Trout Lake  
763 in the Yukon Territory (Irvine et al., 2012) suggest temperatures declined 2-3 °C since  
764 the HTM, somewhat smaller in magnitude, but within the uncertainty of the  $\delta^2 H_{wax}$   
765 inference. At Trout Lake, most of this cooling occurred at 9.6 ka, synchronous to the  
766 stepped  $\delta^2 H_{wax}$  decline at Lake E5. Holocene temperatures were approximately stable at  
767 Burial Lake in northwest Alaska (Kurek et al., 2009a) and at Hanging Lake in the  
768 northern Yukon (Kurek et al., 2009b). The absent or more subtle cooling signal seen in  
769 the chironomids compared to  $\delta^2 H_{wax}$  or beetles could result from limitations in the  
770 various proxy interpretations. Alternatively, reduced temperature variability at Zagoskin  
771 and Burial Lakes have been attributed to their proximity to the ocean (Kurek et al.,  
772 2009a); given the more continental location of Lake E5, this suggests that the interior  
773 regions of eastern Beringia experienced a relatively amplified Holocene cooling  
774 compared to these other sites.

775         The leaf wax  $^2H/^1H$  record from Lake E5 generally agrees with Holocene declines  
776 in lacustrine  $\delta^{18}O$  proxies are recorded at nearby Schrader Pond in Northeast Alaska  
777 (Broadman et al., 2020), as well as a number of sites in southern and central Alaska  
778 (Anderson et al., 2001; Vachula et al., 2017). Broadman et al. (2020) suggest that the  
779 general decrease in  $\delta^{18}O$  values across Alaska is driven in part by expansion of Arctic sea  
780 ice. However, there is a late Holocene increase in cellulose  $\delta^{18}O$  at St. Matthews Island in  
781 the central Bering Sea (Jones et al., 2020), interpreted to result from declining winter ice  
782 cover in the Bering Sea. More records of sea ice are needed to elucidate if Arctic and

783 Bering sea ice histories are decoupled or if the apparent difference results from different  
784 seasonal expressions of the  $\delta^{18}\text{O}$  sea ice response from continental and island sites. The  
785 continental sites, which together document cooling and drying of Beringia climate over  
786 the Holocene, with a particular bias towards summer conditions, contrast with the Lake  
787 E5 alkenone record which records a winter/spring warming signal over the Holocene in  
788 response to increasing cold-season insolation and greenhouse gasses (Longo et al., 2020).  
789 The contrasting wintertime warming signal is regionally corroborated by ice wedge  
790 isotopes in the Yukon (Holland et al., 2020) as well as the retreating winter sea ice cover  
791 in the Bering Sea (Jones et al., 2020). The Lake E5 record shows that after brief warm  
792 periods at  $\sim 5.6 \pm 0.2$  ka and from 4.0 to 3.5 ka, cooling re-intensified from 4 to 0.1 ka,  
793 which is roughly synchronous with the expansion of alpine glaciers in the Brooks Range  
794 (Badding et al., 2013). Temperatures were more stable during over the last 2000 years  
795 (Figure 11), but the median of the monte carlo simulation still exhibits cooling at a rate of  
796  $\sim 0.6 \pm 0.2$  °C per millennium, exceeding the average pan-Arctic late Holocene cooling of  
797  $0.22$  °C per thousand years (Kaufman et al., 2009).



798  
799 **Figure 11.** Lake E5  $\delta^2\text{H}_{\text{wax}}$ -inferred temperature anomalies over the past 1000 years (red,  
800 with smoothing spline) and CRUTEM4 instrumental observations from Northern Alaska  
801 (blue).  
802

803 The Lake E5  $\delta^2\text{H}_{\text{precipitation}}$  record contextualizes ongoing Alaska warming in the  
804 prism of climate changes of the past  $\sim 32$  kyr. Figure 11 shows that modern (coretop) leaf  
805 waxes from the historical era at Lake E5 are  $^2\text{H}$ -enriched relative to the PI average by  $5.2$   
806  $\pm 0.8$  ‰, equating to  $\sim 2^\circ\text{C}$  of warming (Monte Carlo range:  $-1$  to  $+5$  °C). The amplitude

807 of post-industrial warming we reconstruct at Lake E5 is similar to the 2.5°C of JJA  
808 warming apparent in the CRUTEM4 instrumental database for Northern Alaska (Jones et  
809 al., 2012) and the 2 °C rise in mean annual temperature inferred from the nearby McCall  
810 glacier ice core  $^{18}\text{O}/^{16}\text{O}$  ratios (Klein et al., 2015). Furthermore, whereas, Porter et al.  
811 (2019) show, based on  $^{18}\text{O}/^{16}\text{O}$  in ground ice, that recent warming in Central Yukon has  
812 surpassed peak early-Holocene warmth, this is not the case at Lake E5. The  $\delta^{18}\text{O}$  values  
813 in diatoms at nearby Schrader Lake decline during the Holocene but do not exhibit a  
814 reversal to HTM levels (Broadman et al., 2020). Nonetheless, the isotope-inferred  
815 warming at Lake E5, in conjunction with the instrumental observations, indicate that  
816 recent temperature increase in northern Alaska exceeds the +1.4 °C pan-Arctic  
817 temperature change between the pre-industrial period and today (Kaufman et al., 2009).  
818 This amplified warming contrasts with the spatial pattern of temperature change across  
819 the deglaciation, when Beringian warming was smaller than other parts of the Arctic. The  
820 contraction of winter and summer sea ice in the adjacent Chukchi Sea (Serreze et al.,  
821 2007; Stroeve et al., 2012) and the expansion of shrubs into low tundra biomes (Sturm et  
822 al., 2001; Elmendorf et al., 2012; Buchwal et al., 2020) are likely feedbacks amplifying  
823 recent warming in northern Alaska.

824

## 825 **5. Conclusions**

826 A new record of Eastern Beringia paleoclimate provides evidence for a relatively  
827 mild LGM and a series of abrupt climate transitions during the deglacial period, with  
828 rapid warming intervals observed at 19 ka, 14.8 ka, 13.4 and 11.6 ka. Furthermore, data-  
829 model comparisons demonstrate that the magnitude of past Arctic amplification in this  
830 region has evolved from the last glacial period to today. In particular, whereas muted  
831 LGM cooling in Beringia indicates strong ameliorating effects of ice sheet orography and  
832 possibly enhanced continentality, the Holocene and modern changes are amplified  
833 relative to other Arctic sites, which we speculate is due to surface feedbacks including  
834 recent sea ice decline and shrub expansion in conjunction with the removal of factors  
835 such as the LIS which dampened regional temperature change during the deglacial. These  
836 results predict that Arctic Alaskan temperatures will continue to warm more rapidly in  
837 the future than other sectors of the Arctic.



838

839 **Acknowledgments**

840 We thank Rafael Taroza for laboratory assistance. This work is partially supported  
841 by National Geographic grant 9397-13 (Y.H.), and National Science Foundation grants  
842 PLR-1503846 (Y.H., J.M.R.), PLR-1504069 (C.M.) and DEB-1026843 (ARC-LTER),  
843 and DBI-0923571 (J.M.W.) and a National Ocean Sciences Accelerator Mass  
844 Spectroscopy Graduate Student Internship (W.M.L.). A.H.

845

846

847

848 The National Center for Atmospheric Research is sponsored by the NSF.

849

850

851

852

853 **Data availability**

854 Lake E5 leaf wax hydrogen isotope data and precipitation isotope data from the  
855 Toolik Field Station are freely available at the Arctic Data Center Archives. Upon  
856 publication, the sediment record will be archived at the NOAA paleoclimate database,  
857 and this statement will be updated with a DOI accordingly.

858

859 **Competing Interests**

860 The authors declare no competing interests.

861

862 **References**

863 Abbott, M.B., Edwards, M.E., Finney, B.P., 2010. A 40,000-yr record of environmental  
864 change from Burial Lake in Northwest Alaska. *Quatern. Res.* 74, 156-165.

865 Abbott, M.B., Finney, B.P., Edwards, M.E., Kelts, K.R., 2000. Lake-level reconstruction  
866 and paleohydrology of Birch Lake, central Alaska, based on seismic reflection profiles  
867 and core transects. *Quatern. Res.* 53, 154-166.

- 868 Abbott, M.B., Stafford Jr, T.W., 1996. Radiocarbon Geochemistry of Modern and  
869 Ancient Arctic Lake Systems, Baffin Island, Canada. *Quatern. Res.* 45, 300-311.
- 870 Andersen, K.K., Azuma, N., Barnola, J.-M., Bigler, M., Biscaye, P., Caillon, N.,  
871 Chappellaz, J., Clausen, H.B., Dahl-Jensen, D., Fischer, H., 2004. High-resolution record  
872 of Northern Hemisphere climate extending into the last interglacial period. *Nature* 431,  
873 147-151.
- 874 Anderson, L., Abbott, M.B., Finney, B.P., 2001. Holocene climate inferred from oxygen  
875 isotope ratios in lake sediments, central Brooks Range, Alaska. *Quatern. Res.* 55, 313-  
876 321.
- 877 Andersson, R.A., Kuhry, P., Meyers, P., Zebühr, Y., Crill, P., Mörrh, M., 2011. Impacts  
878 of paleohydrological changes on n-alkane biomarker compositions of a Holocene peat  
879 sequence in the eastern European Russian Arctic. *Org. Geochem.* 42, 1065-1075.
- 880 Appleby, P., Nolan, P., Gifford, D., Godfrey, M., Oldfield, F., Anderson, N., Battarbee,  
881 R., 1986.  $^{210}\text{Pb}$  dating by low background gamma counting. *Hydrobiologia* 143, 21-27.
- 882 Appleby, P., Oldfield, F., 1978. The calculation of lead-210 dates assuming a constant  
883 rate of supply of unsupported  $^{210}\text{Pb}$  to the sediment. *Catena* 5, 1-8.
- 884 Atkinson, T.C., Briffa, K.R., Coope, G., 1987. Seasonal temperatures in Britain during  
885 the past 22,000 years, reconstructed using beetle remains. *Nature* 325, 587-592.
- 886 Badding, M.E., Briner, J.P., Kaufman, D.S., 2013.  $^{10}\text{Be}$  ages of late Pleistocene  
887 deglaciation and Neoglaciation in the north - central Brooks Range, Arctic Alaska.  
888 *Journal of Quaternary Science* 28, 95-102.
- 889 Bailey, H.L., Klein, E.S., Welker, J.M., 2019. Synoptic and mesoscale mechanisms drive  
890 winter precipitation  $\delta^{18}\text{O}/\delta^2\text{H}$  in south - central Alaska. *Journal of Geophysical*  
891 *Research: Atmospheres* 124, 4252-4266.
- 892 Bartlein, P., Edwards, M., Hostetler, S., Shafer, S., Anderson, P., Brubaker, L., Lozhkin,  
893 A., 2015. Early-Holocene warming in Beringia and its mediation by sea-level and  
894 vegetation changes. *Climate of the Past Discussions* 11, 873-932.

- 895 Bartlein, P., Harrison, S., Brewer, S., Connor, S., Davis, B., Gajewski, K., Guiot, J.,  
896 Harrison-Prentice, T., Henderson, A., Peyron, O., 2011. Pollen-based continental climate  
897 reconstructions at 6 and 21 ka: a global synthesis. *Climate dynamics* 37, 775-802.
- 898 Berke, M.A., Sierra, A.C., Bush, R., Cheah, D., O'Connor, K., 2019. Controls on leaf  
899 wax fractionation and  $\delta^2\text{H}$  values in tundra vascular plants from western Greenland.  
900 *Geochim. Cosmochim. Acta* 244, 565-583.
- 901 Binford, M.W., 1990. Calculation and uncertainty analysis of  $^{210}\text{Pb}$  dates for PIRLA  
902 project lake sediment cores. *J. Paleolimnol.* 3, 253-267.
- 903 Blaauw, M., 2010. Methods and code for 'classical' age-modelling of radiocarbon  
904 sequences. *quaternary geochronology* 5, 512-518.
- 905 Bray, E., Evans, E., 1961. Distribution of n-paraffins as a clue to recognition of source  
906 beds. *Geochim. Cosmochim. Acta* 22, 2-15.
- 907 Briner, J.P., Kaufman, D.S., 2008. Late Pleistocene mountain glaciation in Alaska: key  
908 chronologies. *Journal of Quaternary Science* 23, 659-670.
- 909 Broadman, E., Kaufman, D.S., Henderson, A.C., Malmierca-Vallet, I., Leng, M.J., Lacey,  
910 J.H., 2020. Coupled impacts of sea ice variability and North Pacific atmospheric  
911 circulation on Holocene hydroclimate in Arctic Alaska. *Proceedings of the National*  
912 *Academy of Sciences* 117, 33034-33042.
- 913 Broccoli, A.J., Manabe, S., 1987. The effects of the Laurentide ice sheet on North  
914 American climate during the last glacial maximum. *Geographie physique et Quaternaire*  
915 41, 9.
- 916 Broecker, W.S., Kennett, J.P., Flower, B.P., Teller, J.T., Trumbore, S., Bonani, G.,  
917 Wolfli, W., 1989. Routing of meltwater from the Laurentide Ice Sheet during the  
918 Younger Dryas cold episode.
- 919 Buchwal, A., Sullivan, P.F., Macias-Fauria, M., Post, E., Myers-Smith, I.H., Stroeve,  
920 J.C., Blok, D., Tape, K.D., Forbes, B.C., Ropars, P., 2020. Divergence of Arctic shrub  
921 growth associated with sea ice decline. *Proceedings of the National Academy of Sciences*  
922 117, 33334-33344.

- 923 Buizert, C., Gkinis, V., Severinghaus, J.P., He, F., Lecavalier, B.S., Kindler, P.,  
924 Leuenberger, M., Carlson, A.E., Vinther, B., Masson-Delmotte, V., 2014. Greenland  
925 temperature response to climate forcing during the last deglaciation. *Science* 345, 1177-  
926 1180.
- 927 Cherry, J.E., Déry, S.J., Stieglitz, M., Pan, F.-f., 2014. Meteorology and climate of Toolik  
928 Lake and the north slope of Alaska: Past, present and future. *Alaska's changing Arctic:  
929 Ecological consequences for tundra, streams, and lakes*. Oxford Univ. Press.
- 930 Chikaraishi, Y., Naraoka, H., 2007.  $\delta^{13}\text{C}$  and  $\delta\text{D}$  relationships among three n-alkyl  
931 compound classes (n-alkanoic acid, n-alkane and n-alkanol) of terrestrial higher plants.  
932 *Org. Geochem.* 38, 198-215.
- 933 Chipman, M.L., Kling, G.W., Lundstrom, C.C., Hu, F.S., 2016. Multiple thermo-  
934 erosional episodes during the past six millennia: Implications for the response of Arctic  
935 permafrost to climate change. *Geology*, G37693. 37691.
- 936 Clark, J., Mitrovica, J.X., Alder, J., 2014. Coastal paleogeography of the California–  
937 Oregon–Washington and Bering Sea continental shelves during the latest Pleistocene and  
938 Holocene: implications for the archaeological record. *Journal of Archaeological Science*  
939 52, 12-23.
- 940 Crump, S.E., Miller, G.H., Power, M., Sepúlveda, J., Dildar, N., Coghlan, M., Bunce, M.,  
941 2019. Arctic shrub colonization lagged peak postglacial warmth: Molecular evidence in  
942 lake sediment from Arctic Canada. *Global Change Biol.* 25, 4244-4256.
- 943 Dahl-Jensen, D., Mosegaard, K., Gundestrup, N., Clow, G.D., Johnsen, S.J., Hansen,  
944 A.W., Balling, N., 1998. Past temperatures directly from the Greenland ice sheet. *Science*  
945 282, 268-271.
- 946 Daniels, W.C., Huang, Y., Russell, J.M., Giblin, A.E., 2018. Effect of continuous light on  
947 leaf wax isotope ratios in *Betula nana* and *Eriophorum vaginatum*: Implications for Arctic  
948 paleoclimate reconstructions. *Org. Geochem.* 125, 70-81.
- 949 Daniels, W.C., Kling, G.W., Giblin, A.E., 2015. Benthic community metabolism in deep  
950 and shallow Arctic lakes during 13 years of whole-lake fertilization. *Limnol. Oceanogr.*,  
951 n/a-n/a.

- 952 Daniels, W.C., Russell, J.M., Giblin, A.E., Welker, J.M., Klein, E.S., Huang, Y., 2017.  
953 Hydrogen isotope fractionation in leaf waxes in the Alaskan Arctic tundra. *Geochim.*  
954 *Cosmochim. Acta* 213, 216-236.
- 955 Dansgaard, W., 1964. Stable isotopes in precipitation. *Tellus* 16, 436-468.
- 956 Denton, G., Alley, R., Comer, G., Broecker, W., 2005. The role of seasonality in abrupt  
957 climate change. *Quaternary Science Reviews* 24, 1159-1182.
- 958 Dion-Kirschner, H., McFarlin, J.M., Masterson, A.L., Axford, Y., Osburn, M.R., 2020.  
959 Modern constraints on the sources and climate signals recorded by sedimentary plant  
960 waxes in west Greenland. *Geochim. Cosmochim. Acta*.
- 961 Dyke, A.S., 2004. An outline of North American deglaciation with emphasis on central  
962 and northern Canada. *Quaternary glaciations: Extent and chronology* 2, 373-424.
- 963 Eisner, W.R., Colinvaux, P.A., 1992. Late Quaternary Pollen Records from Oil Lake and  
964 Feniak Lake, Alaska, U.S.A. *Arct. Alp. Res.* 24, 56-63.
- 965 Elder, C.D., Xu, X., Walker, J., Schnell, J.L., Hinkel, K.M., Townsend-Small, A., Arp,  
966 C.D., Pohlman, J.W., Gaglioti, B.V., Czimeczik, C.I., 2018. Greenhouse gas emissions  
967 from diverse Arctic Alaskan lakes are dominated by young carbon. *Nature Climate*  
968 *Change* 8, 166.
- 969 Elias, S.A., Short, S.K., Nelson, C.H., Birks, H.H., 1996. Life and times of the Bering  
970 land bridge. *Nature* 382, 60-63.
- 971 Elmendorf, S.C., Henry, G.H., Hollister, R.D., Björk, R.G., Boulanger-Lapointe, N.,  
972 Cooper, E.J., Cornelissen, J.H., Day, T.A., Dorrepaal, E., Elumeeva, T.G., 2012. Plot-  
973 scale evidence of tundra vegetation change and links to recent summer warming. *Nature*  
974 *Climate Change* 2, 453.
- 975 England, J.H., Furze, M.F., 2008. New evidence from the western Canadian Arctic  
976 Archipelago for the resubmergence of Bering Strait. *Quatern. Res.* 70, 60-67.
- 977 Engstrom, D., Hansen, B., Wright, H., 1990. A possible Younger Dryas record in  
978 southeastern Alaska. *Science* 250, 1383-1385.

- 979 Epstein, S., 1995. The isotopic climatic records in the Allerød-Bølling-Younger Dryas  
980 and Post-Younger Dryas events. *Global Biogeochem. Cycles* 9, 557-563.
- 981 Feakins, S.J., 2013. Pollen-corrected leaf wax D/H reconstructions of northeast African  
982 hydrological changes during the late Miocene. *Palaeogeogr., Palaeoclimatol., Palaeoecol.*  
983 374, 62-71.
- 984 Gaglioti, B.V., Mann, D.H., Wooller, M.J., Jones, B.M., Wiles, G.C., Groves, P., Kunz,  
985 M.L., Baughman, C.A., Reanier, R.E., 2017. Younger-Dryas cooling and sea-ice  
986 feedbacks were prominent features of the Pleistocene-Holocene transition in Arctic  
987 Alaska. *Quaternary Science Reviews* 169, 330-343.
- 988 Gao, L., Edwards, E.J., Zeng, Y., Huang, Y., 2014. Major Evolutionary Trends in  
989 Hydrogen Isotope Fractionation of Vascular Plant Leaf Waxes. *PLoS ONE* 9, e112610.
- 990 Goebel, T., Waters, M.R., O'rourke, D.H., 2008. The late Pleistocene dispersal of modern  
991 humans in the Americas. *science* 319, 1497-1502.
- 992 Graf, K.E., Bigelow, N.H., 2011. Human response to climate during the Younger Dryas  
993 chronozone in central Alaska. *Quaternary International* 242, 434-451.
- 994 Grootes, P., Stuiver, M., 1997. Oxygen 18/16 variability in Greenland snow and ice with  
995 10– 3 - to 105 - year time resolution. *Journal of Geophysical Research: Oceans* (1978–  
996 2012) 102, 26455-26470.
- 997 Grootes, P., Stuiver, M., White, J., Johnson, S., Jouzel, J., 1993. Comparison of oxygen  
998 isotope records from the GISP2 and GRIP Greenland ice cores. *Nature* 366, 3.
- 999 Hamilton, T.D., 2003. Glacial Geology of the Toolik Lake and Upper Kuparuk River  
1000 Regions, in: Walker, D. (Ed.), *Biological Papers of the University of Alaska. Institute of*  
1001 *Arctic Biology*, Fairbanks, Alaska.
- 1002 Holland, K.M., Porter, T.J., Froese, D.G., Kokelj, S.V., Buchanan, C.A., 2020. Ice-  
1003 Wedge Evidence of Holocene Winter Warming in the Canadian Arctic. *Geophys. Res.*  
1004 *Lett.* 47, e2020GL087942.
- 1005 Hu, A., Meehl, G.A., Han, W., Abe - Ouchi, A., Morrill, C., Okazaki, Y., Chikamoto,  
1006 M.O., 2012. The Pacific - Atlantic seesaw and the Bering Strait. *Geophys. Res. Lett.* 39.

1007 Hu, A., Meehl, G.A., Han, W., Otto-Blietner, B., Abe-Ouchi, A., Rosenbloom, N., 2015.  
1008 Effects of the Bering Strait closure on AMOC and global climate under different  
1009 background climates. *Prog. Oceanogr.* 132, 174-196.

1010 Hu, F.S., Nelson, D.M., Clarke, G.H., Rühland, K.M., Huang, Y., Kaufman, D.S., Smol,  
1011 J.P., 2006. Abrupt climatic events during the last glacial - interglacial transition in  
1012 Alaska. *Geophys. Res. Lett.* 33.

1013 Irvine, F., Cwynar, L.C., Vermaire, J.C., Rees, A.B., 2012. Midge-inferred temperature  
1014 reconstructions and vegetation change over the last~ 15,000 years from Trout Lake,  
1015 northern Yukon Territory, eastern Beringia. *J. Paleolimnol.* 48, 133-146.

1016 Jakobsson, M., Pearce, C., Cronin, T.M., Backman, J., Anderson, L.G., Barrientos, N.,  
1017 Björk, G., Coxall, H., De Boer, A., Mayer, L.A., 2017. Post-glacial flooding of the  
1018 Bering Land Bridge dated to 11 cal ka BP based on new geophysical and sediment  
1019 records. *Climate of the Past* 13, 991.

1020 Jespersen, R.G., Leffler, A.J., Oberbauer, S.F., Welker, J.M., 2018. Arctic plant  
1021 ecophysiology and water source utilization in response to altered snow: isotopic ( $\delta^{18}\text{O}$   
1022 and  $\delta^2\text{H}$ ) evidence for meltwater subsidies to deciduous shrubs. *Oecologia* 187, 1009-  
1023 1023.

1024 Johnsen, S.J., Clausen, H.B., Dansgaard, W., Fuhrer, K., Gundestrup, N., Hammer, C.U.,  
1025 Iversen, P., Jouzel, J., Stauffer, B., Steffensen, J.P., 1992. Irregular glacial interstadials  
1026 recorded in a new Greenland ice core. *Nature* 359, 3.

1027 Jones, M.C., Berkelhammer, M., Keller, K.J., Yoshimura, K., Wooller, M.J., 2020. High  
1028 sensitivity of Bering Sea winter sea ice to winter insolation and carbon dioxide over the  
1029 last 5500 years. *Science advances* 6, eaaz9588.

1030 Jones, M.C., Yu, Z., 2010. Rapid deglacial and early Holocene expansion of peatlands in  
1031 Alaska. *Proceedings of the National Academy of Sciences* 107, 7347-7352.

1032 Jones, P.D., Lister, D.H., Osborn, T.J., Harpham, C., Salmon, M., Morice, C.P., 2012.  
1033 Hemispheric and large-scale land-surface air temperature variations: An extensive  
1034 revision and an update to 2010. *Journal of Geophysical Research: Atmospheres* 117, n/a-  
1035 n/a.

- 1036 Kaufman, D., 2004. Holocene thermal maximum in the western Arctic (0–180°W).  
1037 Quaternary Science Reviews 23, 529-560.
- 1038 Kaufman, D.S., Schneider, D.P., McKay, N.P., Ammann, C.M., Bradley, R.S., Briffa,  
1039 K.R., Miller, G.H., Otto-Bliesner, B.L., Overpeck, J.T., Vinther, B.M., 2009. Recent  
1040 warming reverses long-term arctic cooling. Science 325, 1236-1239.
- 1041 Keigwin, L.D., Donnelly, J.P., Cook, M.S., Driscoll, N.W., Brigham-Grette, J., 2006.  
1042 Rapid sea-level rise and Holocene climate in the Chukchi Sea. Geology 34, 861-864.
- 1043 Keisling, B.A., Castañeda, I.S., Brigham-Grette, J., 2017. Hydrological and temperature  
1044 change in Arctic Siberia during the intensification of Northern Hemisphere Glaciation.  
1045 Earth. Planet. Sci. Lett. 457, 136-148.
- 1046 Kienast, S.S., McKay, J.L., 2001. Sea surface temperatures in the subarctic northeast  
1047 Pacific reflect millennial - scale climate oscillations during the last 16 kyrs. Geophys.  
1048 Res. Lett. 28, 1563-1566.
- 1049 Klein, E.S., Nolan, M., McConnell, J., Sigl, M., Cherry, J., Young, J., Welker, J.M.,  
1050 2015. McCall Glacier record of Arctic climate change: Interpreting a northern Alaska ice  
1051 core with regional water isotopes. Quaternary Science Reviews.
- 1052 Köhler, P., Nehrbass-Ahles, C., Schmitt, J., Stocker, T.F., Fischer, H., 2017. A 156 kyr  
1053 smoothed history of the atmospheric greenhouse gases CO<sub>2</sub>, CH<sub>4</sub>, and N<sub>2</sub>O and their  
1054 radiative forcing. Earth System Science Data 9, 363-387.
- 1055 Kokorowski, H., Anderson, P., Mock, C., Lozhkin, A., 2008. A re-evaluation and spatial  
1056 analysis of evidence for a Younger Dryas climatic reversal in Beringia. Quaternary  
1057 Science Reviews 27, 1710-1722.
- 1058 Konecky, B., Russell, J., Bijaksana, S., 2016. Glacial aridity in central Indonesia coeval  
1059 with intensified monsoon circulation. Earth. Planet. Sci. Lett. 437, 15-24.
- 1060 Kühn, H., Lembke-Jene, L., Gersonde, R., Esper, O., Lamy, F., Arz, H., Kuhn, G.,  
1061 Tiedemann, R., 2014. Laminated sediments in the Bering Sea reveal atmospheric  
1062 teleconnections to Greenland climate on millennial to decadal timescales during the last  
1063 deglaciation. Climate of the Past 10, 2215-2236.



- 1064 Kurek, J., Cwynar, L.C., Ager, T.A., Abbott, M.B., Edwards, M.E., 2009a. Late  
1065 Quaternary paleoclimate of western Alaska inferred from fossil chironomids and its  
1066 relation to vegetation histories. *Quaternary Science Reviews* 28, 799-811.
- 1067 Kurek, J., Cwynar, L.C., Vermaire, J.C., 2009b. A late Quaternary paleotemperature  
1068 record from Hanging Lake, northern Yukon Territory, eastern Beringia. *Quatern. Res.* 72,  
1069 246-257.
- 1070 Lachniet, M.S., Lawson, D.E., Stephen, H., Sloat, A.R., Patterson, W.P., 2016. Isoscapes  
1071 of  $\delta^{18}\text{O}$  and  $\delta^2\text{H}$  reveal climatic forcings on Alaska and Yukon precipitation. *Water*  
1072 *Resour. Res.* 52, 6575-6586.
- 1073 Ladd, S.N., Maloney, A.E., Nelson, D.B., Prebble, M., Camperio, G., Sear, D.A., Hassall,  
1074 J.D., Langdon, P.G., Sachs, J.P., Dubois, N., 2021. Leaf Wax Hydrogen Isotopes as a  
1075 Hydroclimate Proxy in the Tropical Pacific. *Journal of Geophysical Research:*  
1076 *Biogeosciences* 126, e2020JG005891.
- 1077 Laskar, J., Robutel, P., Joutel, F., Gastineau, M., Correia, A., Levrard, B., 2004. A long-  
1078 term numerical solution for the insolation quantities of the Earth. *Astronomy &*  
1079 *Astrophysics* 428, 261-285.
- 1080 Li, C., Battisti, D.S., Schrag, D.P., Tziperman, E., 2005. Abrupt climate shifts in  
1081 Greenland due to displacements of the sea ice edge. *Geophys. Res. Lett.* 32.
- 1082 Lisiecki, L.E., Raymo, M.E., 2005. A Pliocene - Pleistocene stack of 57 globally  
1083 distributed benthic  $\delta^{18}\text{O}$  records. *Paleoceanography* 20.
- 1084 Liu, Z., Otto-Bliesner, B., He, F., Brady, E., Tomas, R., Clark, P., Carlson, A., Lynch-  
1085 Stieglitz, J., Curry, W., Brook, E., 2009. Transient simulation of last deglaciation with a  
1086 new mechanism for Bølling-Allerød warming. *Science* 325, 310-314.
- 1087 Liu, Z., Wen, X., Brady, E., Otto-Bliesner, B., Yu, G., Lu, H., Cheng, H., Wang, Y.,  
1088 Zheng, W., Ding, Y., 2014. Chinese cave records and the East Asia summer monsoon.  
1089 *Quaternary Science Reviews* 83, 115-128.
- 1090 Livingstone, D., 1955. Some pollen profiles from arctic Alaska. *Ecology*, 587-600.

- 1091 L fverstr m, M., Liakka, J., 2016. On the limited ice intrusion in Alaska at the LGM.  
1092 Geophys. Res. Lett. 43, 11,030-011,038.
- 1093 Longo, W.M., Huang, Y., Russell, J.M., Morrill, C., Daniels, W.C., Giblin, A.E.,  
1094 Crowther, J., 2020. Insolation and greenhouse gases drove Holocene winter and spring  
1095 warming in Arctic Alaska. Quaternary Science Reviews 242, 106438.
- 1096 Longo, W.M., Theroux, S., Giblin, A.E., Zheng, Y., Dillon, J.T., Huang, Y., 2016.  
1097 Temperature calibration and phylogenetically distinct distributions for freshwater  
1098 alkenones: Evidence from northern Alaskan lakes. Geochim. Cosmochim. Acta 180, 177-  
1099 196.
- 1100 Lynch, A., Chapin III, F., Hinzman, L., Wu, W., Lilly, E., Vourlitis, G., Kim, E., 1999.  
1101 Surface energy balance on the arctic tundra: Measurements and models. J. Clim. 12.
- 1102 Maier, E., Zhang, X., Abelman, A., Gersonde, R., Mulitza, S., Werner, M., M  heust,  
1103 M., Ren, J., Chaplign, B., Meyer, H., Stein, R., Tiedemann, R., Lohmann, G., 2018.  
1104 North Pacific freshwater events linked to changes in glacial ocean circulation. Nature  
1105 559, 241-245.
- 1106 Mangerud, J., Briner, J.P., Goslar, T., Svendsen, J.I., 2017. The B  lling - age Blomv  g  
1107 Beds, western Norway: implications for the Older Dryas glacial re - advance and the age  
1108 of the deglaciation. Boreas 46, 162-184.
- 1109 Manley, W.F., Kaufman, D., 2002. Alaska paleoglacier atlas. Institute of Arctic and  
1110 Alpine Research (INSTAAR), University of Colorado, Boulder, CO.
- 1111 Mann, D.H., Groves, P., Kunz, M.L., Reanier, R.E., Gaglioti, B.V., 2013. Ice-age  
1112 megafauna in Arctic Alaska: extinction, invasion, survival. Quaternary Science Reviews  
1113 70, 91-108.
- 1114 Mann, D.H., Groves, P., Reanier, R.E., Kunz, M.L., 2010. Floodplains, permafrost,  
1115 cottonwood trees, and peat: What happened the last time climate warmed suddenly in  
1116 arctic Alaska? Quaternary Science Reviews 29, 3812-3830.
- 1117 Mann, D.H., Peteet, D.M., Reanier, R.E., Kunz, M.L., 2002. Responses of an arctic  
1118 landscape to Lateglacial and early Holocene climatic changes: the importance of  
1119 moisture. Quaternary Science Reviews 21, 997-1021.

- 1120 Mann, D.H., Reanier, R.E., Peteet, D.M., Kunz, M.L., Johnson, M., 2001. Environmental  
1121 change and arctic paleoindians. *Arctic Anthropology*, 119-138.
- 1122 McFarlin, J.M., Axford, Y., Masterson, A.L., Osburn, M.R., 2019. Calibration of modern  
1123 sedimentary  $\delta^2\text{H}$  plant wax-water relationships in Greenland lakes. *Quaternary Science*  
1124 *Reviews* 225, 105978.
- 1125 McManus, J.F., Francois, R., Gherardi, J.M., Keigwin, L.D., Brown-Leger, S., 2004.  
1126 Collapse and rapid resumption of Atlantic meridional circulation linked to deglacial  
1127 climate changes. *Nature (London)* 428, 834.
- 1128 Mellat, M., Mustonen, K.-R., Bailey, H.L., Klein, E.S., Marttila, H., Welker, J.M.,  
1129 Submitted. Pan-Arctic summer moisture sources revealed using an event-based  
1130 precipitation isotope ( $\delta^{18}\text{O}$ ,  $\delta^2\text{H}$ , d-excess) network (PAPIN. *Earth. Planet. Sci. Lett.*
- 1131 Melles, M., Brigham-Grette, J., Minyuk, P.S., Nowaczyk, N.R., Wennrich, V., DeConto,  
1132 R.M., Anderson, P.M., Andreev, A.A., Coletti, A., Cook, T.L., Haltia-Hovi, E.,  
1133 Kukkonen, M., Lozhkin, A.V., Rosén, P., Tarasov, P., Vogel, H., Wagner, B., 2012. 2.8  
1134 Million Years of Arctic Climate Change from Lake El'gygytgyn, NE Russia. *Science*  
1135 337, 315-320.
- 1136 Meyer, H., Schirrmeister, L., Yoshikawa, K., Opel, T., Wetterich, S., Hubberten, H.W.,  
1137 Brown, J., 2010. Permafrost evidence for severe winter cooling during the Younger  
1138 Dryas in northern Alaska. *Geophys. Res. Lett.* 37.
- 1139 Miller, G.H., Alley, R.B., Brigham-Grette, J., Fitzpatrick, J.J., Polyak, L., Serreze, M.C.,  
1140 White, J.W.C., 2010. Arctic amplification: can the past constrain the future? *Quaternary*  
1141 *Science Reviews* 29, 1779-1790.
- 1142 Nichols, J.E., Peteet, D.M., Moy, C.M., Castañeda, I.S., McGeachy, A., Perez, M., 2014.  
1143 Impacts of climate and vegetation change on carbon accumulation in a south-central  
1144 Alaskan peatland assessed with novel organic geochemical techniques. *The Holocene* 24,  
1145 1146-1155.
- 1146 O'Connor, K.F., Berke, M.A., Ziolkowski, L.A., 2020. Hydrogen isotope fractionation in  
1147 modern plants along a boreal-tundra transect in Alaska. *Geochem. Org.* 147, 104064.

- 1148 Okazaki, Y., Timmermann, A., Menviel, L., Harada, N., Abe-Ouchi, A., Chikamoto, M.,  
1149 Mouchet, A., Asahi, H., 2010. Deepwater formation in the North Pacific during the last  
1150 glacial termination. *Science* 329, 200-204.
- 1151 Oswald, W.W., Anderson, P.M., Brown, T.A., Brubaker, L.B., Hu, F.S., Lozhkin, A.V.,  
1152 Tinner, W., Kaltenrieder, P., 2005. Effects of sample mass and macrofossil type on  
1153 radiocarbon dating of arctic and boreal lake sediments. *The Holocene* 15, 758-767.
- 1154 Oswald, W.W., Brubaker, L.B., Anderson, P.M., 1999. Late Quaternary vegetational  
1155 history of the Howard Pass area, northwestern Alaska. *Canadian Journal of Botany* 77,  
1156 570-581.
- 1157 Otto-Bliesner, B.L., Brady, E.C., Clauzet, G., Tomas, R., Levis, S., Kothavala, Z., 2006.  
1158 Last glacial maximum and Holocene climate in CCSM3. *J. Clim.* 19, 2526-2544.
- 1159 Pautler, B.G., Reichert, G.-J., Sanborn, P.T., Simpson, M.J., Weijers, J.W., 2014.  
1160 Comparison of soil derived tetraether membrane lipid distributions and plant-wax  $\delta D$   
1161 compositions for reconstruction of Canadian Arctic temperatures. *Palaeogeogr.,*  
1162 *Palaeoclimatol., Palaeoecol.* 404, 78-88.
- 1163 Pendleton, S.L., Ceperley, E.G., Briner, J.P., Kaufman, D.S., Zimmerman, S., 2015.  
1164 Rapid and early deglaciation in the central Brooks Range, Arctic Alaska. *Geology* 43,  
1165 419-422.
- 1166 Pico, T., Mitrovica, J., Mix, A., 2020. Sea level fingerprinting of the Bering Strait  
1167 flooding history detects the source of the Younger Dryas climate event. *Science advances*  
1168 6, eaay2935.
- 1169 Porter, T.J., Froese, D.G., Feakins, S.J., Bindeman, I.N., Mahony, M.E., Pautler, B.G.,  
1170 Reichert, G.-J., Sanborn, P.T., Simpson, M.J., Weijers, J.W.H., 2016. Multiple water  
1171 isotope proxy reconstruction of extremely low last glacial temperatures in Eastern  
1172 Beringia (Western Arctic). *Quaternary Science Reviews* 137, 113-125.
- 1173 Porter, T.J., Schoenemann, S.W., Davies, L.J., Steig, E.J., Bandara, S., Froese, D.G.,  
1174 2019. Recent summer warming in northwestern Canada exceeds the Holocene thermal  
1175 maximum. *Nature communications* 10, 1631.
- 1176 Praetorius, S.K., Mix, A.C., 2014. Synchronization of North Pacific and Greenland  
1177 climates preceded abrupt deglacial warming. *Science* 345, 444-448.

- 1178 Putman, A.L., Feng, X., Sonder, L.J., Posmentier, E.S., 2017. Annual variation in event-  
1179 scale precipitation  $\delta^2\text{H}$  at Barrow, AK, reflects vapor source region. *Atmospheric*  
1180 *chemistry and Physics* 17, 4627-4639.
- 1181 Rae, J.W., Gray, W., Wills, R., Eisenman, I., Fitzhugh, B., Fotheringham, M., Little, E.,  
1182 Rafter, P., Rees-Owen, R., Ridgwell, A., 2020. Overturning circulation, nutrient  
1183 limitation, and warming in the Glacial North Pacific. *Science advances* 6, eabd1654.
- 1184 Reimer, P.J., Bard, E., Bayliss, A., Beck, J.W., Blackwell, P.G., Bronk Ramsey, C.,  
1185 Buck, C.E., Cheng, H., Edwards, R.L., Friedrich, M., 2013. IntCal13 and Marine13  
1186 radiocarbon age calibration curves 0-50,000 years cal BP.
- 1187 Sachse, D., Billault, I., Bowen, G.J., Chikaraishi, Y., Dawson, T.E., Feakins, S.J.,  
1188 Freeman, K.H., Magill, C.R., McInerney, F.A., Van der Meer, M.T., 2012. Molecular  
1189 paleohydrology: interpreting the hydrogen-isotopic composition of lipid biomarkers from  
1190 photosynthesizing organisms. *Annual Review of Earth and Planetary Sciences* 40, 221-  
1191 249.
- 1192 Sarnthein, M., Kiefer, T., Grootes, P.M., Elderfield, H., Erlenkeuser, H., 2006. Warmings  
1193 in the far northwestern Pacific promoted pre-Clovis immigration to America during  
1194 Heinrich event 1. *Geology* 34, 141-144.
- 1195 Schmidt, G.A., Bigg, G.R., Rohling, E.J., 1999. Global Seawater Oxygen-18 Database -  
1196 v1.21.
- 1197 Schrag, D.P., Hampt, G., Murray, D.W., 1996. Pore Fluid Constraints on the Temperature  
1198 and Oxygen Isotopic Composition of the Glacial Ocean. *Science* 272, 1930.
- 1199 Serreze, M.C., Holland, M.M., Stroeve, J., 2007. Perspectives on the Arctic's shrinking  
1200 sea-ice cover. *science* 315, 1533-1536.
- 1201 Severinghaus, J.P., Brook, E.J., 1999. Abrupt climate change at the end of the last glacial  
1202 period inferred from trapped air in polar ice. *Science* 286, 930-934.
- 1203 Shah Walter, S.R., Gagnon, A.R., Roberts, M.L., McNichol, A.P., Gaylord, M.C.L.,  
1204 Klein, E., 2015. Ultra-small graphitization reactors for ultra-microscale  $^{14}\text{C}$  analysis at  
1205 the National Ocean Sciences Accelerator Mass Spectrometry (NOSAMS) Facility.  
1206 *Radiocarbon* 57, 109-122.

- 1207 Shakun, J.D., Carlson, A.E., 2010. A global perspective on Last Glacial Maximum to  
1208 Holocene climate change. *Quaternary Science Reviews* 29, 1801-1816.
- 1209 Stabeno, P.J., Schumacher, J.D., Ohtani, K., 1999. The physical oceanography of the  
1210 Bering Sea: A summary of physical, chemical, and biological characteristics, and a  
1211 synopsis of research on the Bering Sea, in: Laughlin, T.R., Ohtani, K. (Eds.), *Dynamics*  
1212 *of the Bering Sea*. TR Loughlin and K. Ohtani (eds.), North Pacific Marine Science  
1213 Organization ....
- 1214 Stroeve, J.C., Kattsov, V., Barrett, A., Serreze, M., Pavlova, T., Holland, M., Meier,  
1215 W.N., 2012. Trends in Arctic sea ice extent from CMIP5, CMIP3 and observations.  
1216 *Geophys. Res. Lett.* 39.
- 1217 Sturm, M., Racine, C., Tape, K., 2001. Climate change: increasing shrub abundance in  
1218 the Arctic. *Nature* 411, 546-547.
- 1219 Tharammal, T., Paul, A., Merkel, U., Noone, D., 2013. Influence of Last Glacial  
1220 Maximum boundary conditions on the global water isotope distribution in an atmospheric  
1221 general circulation model. *Climate of the Past* 9, 789.
- 1222 Thomas, E.K., Clemens, S.C., Prell, W.L., Herbert, T.D., Huang, Y., Liu, Z., Sinninghe  
1223 Damsté, J.S., Sun, Y., Wen, X., 2014. Temperature and leaf wax  $\delta^2\text{H}$  records  
1224 demonstrate seasonal and regional controls on Asian monsoon proxies. *Geology* 42,  
1225 1075-1078.
- 1226 Thomas, E.K., McGrane, S., Briner, J.P., Huang, Y., 2012. Leaf wax  $\delta^2\text{H}$  and varve-  
1227 thickness climate proxies from proglacial lake sediments, Baffin Island, Arctic Canada. *J.*  
1228 *Paleolimnol.*, 1-15.
- 1229 Tierney, J.E., Zhu, J., King, J., Malevich, S.B., Hakim, G.J., Poulsen, C.J., 2020. Glacial  
1230 cooling and climate sensitivity revisited. *Nature* 584, 569-573.
- 1231 Toolik Environmental Data Center Team, 2016. Meteorological monitoring program at  
1232 Toolik, Alaska. Toolik Field Station, Institute of Arctic Biology, University of Alaska  
1233 Fairbanks.
- 1234 Toolik GIS, 2019. Toolik Field Station Bathymetry, in: Sensing, T.F.S.G.a.R. (Ed.).

- 1235 Vachula, R.S., Chipman, M.L., Hu, F.S., 2017. Holocene climatic change in the Alaskan  
1236 Arctic as inferred from oxygen-isotope and lake-sediment analyses at Wahoo Lake. The  
1237 Holocene.
- 1238 Vachula, R.S., Huang, Y., Longo, W.M., Dee, S.G., Daniels, W.C., Russell, J.M., 2019.  
1239 Evidence of Ice Age humans in eastern Beringia suggests early migration to North  
1240 America. *Quaternary Science Reviews* 205, 35-44.
- 1241 Viau, A., Gajewski, K., Sawada, M., Bunbury, J., 2008. Low-and high-frequency climate  
1242 variability in eastern Beringia during the past 25 000 years. *Canadian Journal of Earth  
1243 Sciences* 45, 1435-1453.
- 1244 Welker, J., 2000. Isotopic ( $\delta^{18}\text{O}$ ) characteristics of weekly precipitation collected across  
1245 the USA: an initial analysis with application to water source studies. *Hydrological  
1246 Processes* 14, 1449-1464.
- 1247 Welker, J.M., 2012. ENSO effects on  $\delta^{18}\text{O}$ ,  $\delta^2\text{H}$  and d - excess values in precipitation  
1248 across the US using a high - density, long - term network (USNIP). *Rapid Commun.  
1249 Mass Spectrom.* 26, 1893-1898.
- 1250 Welker, J.M., Rayback, S., Henry, G.H., 2005. Arctic and North Atlantic Oscillation  
1251 phase changes are recorded in the isotopes ( $\delta^{18}\text{O}$  and  $\delta^{13}\text{C}$ ) of *Cassiope tetragona*  
1252 plants. *Global Change Biol.* 11, 997-1002.
- 1253 Wetterich, S., Rudaya, N., Tumskoy, V., Andreev, A.A., Opel, T., Schirrmeister, L.,  
1254 Meyer, H., 2011. Last Glacial Maximum records in permafrost of the East Siberian  
1255 Arctic. *Quaternary Science Reviews* 30, 3139-3151.
- 1256 Wilkie, K., Chaplignin, B., Meyer, H., Burns, S., Petsch, S., Brigham-Grette, J., 2012.  
1257 Modern isotope hydrology and controls on  $\delta\text{D}$  of plant leaf waxes at Lake El'gygytgyn,  
1258 NE Russia. *Climate of the Past Discussions* 8, 3719-3764.
- 1259 Wooller, M.J., Pohlman, J.W., Gaglioti, B.V., Langdon, P., Jones, M., Anthony, K.M.W.,  
1260 Becker, K.W., Hinrichs, K.-U., Elvert, M., 2012. Reconstruction of past methane  
1261 availability in an Arctic Alaska wetland indicates climate influenced methane release  
1262 during the past~ 12,000 years. *J. Paleolimnol.* 48, 27-42.

- 1263 Yang, H., Huang, Y., 2003. Preservation of lipid hydrogen isotope ratios in Miocene  
1264 lacustrine sediments and plant fossils at Clarkia, northern Idaho, USA. *Org. Geochem.*  
1265 34, 413-423.
- 1266 Young, N.E., Briner, J.P., Schaefer, J., Zimmerman, S., Finkel, R.C., 2019. Early  
1267 Younger Dryas glacier culmination in southern Alaska: Implications for North Atlantic  
1268 climate change during the last deglaciation. *Geology* 47, 550-554.
- 1269 Zimov, S., Zimov, N., Tikhonov, A., Chapin, F., 2012. Mammoth steppe: a high-  
1270 productivity phenomenon. *Quaternary Science Reviews* 57, 26-45.  
1271  
1272  
1273